Examensarbete vid Institutionen för geovetenskaper
ISSN 1650-6553 Nr 123

Effects of Upwelling Events on the Atmosphere

Susanna Hagelin

Abstract

During an upwelling event the cold bottom-water is brought to the sea surface. This cools the atmosphere from below and the stratification becomes more stable. When the atmosphere is more stable the turbulence is reduced and, as a consequence, so are the turbulent fluxes.

This study is investigating four periods of upwelling from the Östergarnsholm-site, in the Baltic Sea east of Gotland, during the summer of 2005. The air measurements are taken at a tower at the southernmost tip of Östergarnsholm while the measurements in the water are from a buoy moored 1 km south-southeast of the tower. During all the upwelling events the wind is south-westerly, along the coast of Gotland. This means that the buoy is not within the flux footprint area and is perhaps not always representative of what happens there.

All the periods show a stabilization of the atmosphere as the SST (Sea Surface Temperature) decreases. The heat fluxes, especially the latent heat flux, decreases as the SST decreases.

The amount of CO_2 in the atmosphere, in the summer, is usually higher than the amount in the surface water of the seas because the oceans are a net sink of CO_2. The air-sea flux of CO_2 is to a large extent controlled by this difference. Therefore the flux of CO_2 is usually directed to the sea. The deep-water contains more CO_2 than the surface water because the phytoplankton near the surface removes CO_2 through photosynthesis. The deep-water is also colder and can solve more CO_2. During an upwelling event this CO_2-rich water is brought to the surface. As an upwelling event progresses the difference in CO_2-concentration between the air and the sea is reduced, sometimes reversed, and the flux decreases. This is what happens in three of the investigated periods in this study. During the fourth period a counter gradient flux is observed.

Sammanfattning

När en uppvällning inträffar förs kallt djupvatten upp till havsytan. Det kalla vattnet kyler atmosfären nedifrån, något som leder till mer stabil skiktning. När atmosfären blir mer stabilt skiktad dämpas turbulensen och det medför att de turbulenta flödena också avtar.

I den här studien analyseras fyra perioder med uppvällning. Mätningarna kommer från Östergarnsholm, öster om Gotland, under sommaren 2005. Mätningarna i luften är tagna från en mast vid Östergarnsholms södra udde. Mätningarna i vattnet kommer från en boj som är förankrad 1 km sydsydöst om masten. Vid samtliga uppvällnings-perioder i den här studien är vinden sydvästlig (längs Gotlandskusten). Det betyder att bojen inte befinner sig inom flödenas footprint-area och dess mätningar är kanske inte hela tiden representativa för vad som händer i footprint-arean.

Samtliga undersökta perioder visar på en stabilisering av atmosfären då havsytans temperatur avtar. Värmeflödena, i synnerhet det latenta värmeflödet, avtar i samband med att temperaturen i havsytan sjunker.

Halten av CO_2 i atmosfären är vanligtvis högre än halten i havens ytvatten (under sommaren) eftersom de är en nettosänka för CO_2 globalt sett. CO_2-flödet mellan havsytan och atmosfären styr till en stor del av denna skillnaden i CO_2-halt. Det innebär att CO_2-flödet är riktat neråt, mot havet. Havens djupvatten innehåller mer CO_2 därför att växtplankton nära ytan reducerar CO_2-halten genom fotosyntesen. Djupvattnet är också kallare och kan därför lösa mer CO_2. Under en uppvällning förs detta CO_2-rika vatten upp till ytan. När en uppvällning fortskrider minskar skillnaden i CO_2-halt mellan hav och atmosfär (ibland kan CO_2-halten i ytvattnet även komma att överstiga atmosfärens halt) och flödet avtar. Tre av perioderna i den här studien visar på ett avtagande flöde. Den fjärde perioden uppvisar ett flöde motriktat CO_2-gradienten.

Table of contents

1 Introduction

We live on a planet where the surface is covered by 70% of water. Therefore the importance of understanding how the oceans and the atmosphere interact should not be underestimated. The sea surface does not interact with the atmosphere in the same way as the land surfaces do. Relations that are valid over land must not also hold true over the sea.

The major part of the Earth's carbon is solved in the oceans. They are a net sink in the global atmospheric cycle of carbon dioxide (CO_2). The level of CO_2 in the atmosphere is higher than in the surface waters. In the attempt to reach equilibrium with the CO_2-levels in the atmosphere much of the CO_2 is solved into the oceans. Biological activity also contributes to the absorption of CO_2. Phytoplankton living near or at the surface removes CO_2 from the atmosphere through their photosynthesis. The CO_2 they fixate is not returned to the atmosphere. When they die the gravitation forces them to sink to the ocean floor as detritus[1].

Most oceans are a net sink of CO_2, but not all. The Baltic Sea is a net sink during the year, (Thomas and Schneider, 1999). It's a weak source at winter but during the summer, it's a strong sink for atmospheric CO_2.

During an upwelling event the CO_2-rich bottom-water is brought to the surface and the upwelling region will act as a net source of CO_2. The bottom-water is also rich in nutrients and may cause an increase in primary production that will significantly reduce the amount of CO_2. Which process that is dominant needs to be determined for each region, (Hales et al., 2005; Álvarez et al., 1999).

There are few studies conducting short-term measurements of the effects of an upwelling event on the atmosphere. Most concentrate on the monthly averages of the changes in air-sea flux of CO_2 and how the upwelling affects the local plankton population, see for example Le Borgne et al. (2002) or Astor et al. (2005). One exception is Gago et al. (2003) who conducted a study of the short-term variability of the surface water fugacity[2] of CO_2 and the air-sea fluxes of CO_2 in the upwelling system in the Ría de Vigo in northwest Spain. Their measurements were taken from five cruises in different seasons aboard the R/V Mytilus. They concluded that the fugacity of CO_2 in the Ría is more dependent on biological processes during the summer and fall, but during the winter the temperature was the main factor controlling the fugacity. In the summer (the upwelling season) the Ría is a net sink for CO_2 due to intense biological activity. Álvarez et al. (1999) came to the same conclusion when they studied the seasonal variability of CO_2-fluxes in the Ría de Vigo.

[1] Inorganic or organic debris.

[2] The fugacity of a gas is a measure of its tendency to escape or expand isothermally. The fugacity is the pressure value needed at a given temperature to make the properties of a non-ideal gas to satisfy the equations of an ideal gas.

The purpose of this study is to investigate the effects an upwelling event has on the atmosphere. When cold water is brought up to the sea surface the atmosphere is cooled from below. This should stabilize the atmosphere and reduce the turbulence. This would imply that the turbulent fluxes are damped.

In order to study these effects measurements taken at the Östergarnsholm-site, east of Gotland in the Baltic Sea, in the summer of 2005 are analyzed. The measurements in the air are taken from a measuring tower at the south end of Östergarnsholm. The SST (Sea Surface Temperature) and the level of CO_2 in the water are measured from a buoy 1 km south-southeast of the tower.

This study focuses on the physical factors controlling the air-sea exchange of CO_2.

2 Theory

2.1 Upwelling

Most upwelling situations are wind driven. A wind blowing to the right of a coastline (to the left in the Southern Hemisphere) can result in an upwelling event because the wind generates a net transport of sea water away from the coast. The other major cause is the ocean currents. In the major ocean gyres the flow of the water will cause divergence regions where the surface water for continuity reasons must be replaced with water from below. Ocean currents along the coasts of continents also cause upwelling, for the same reason, particularly at the west coasts of continents. The most famous example being the upwelling region on the west coast of South America, which is affected by the el Niño southern oscillation (ENSO) phenomenon.

This study concerns only wind-driven coastal upwelling. Therefore only that process will be described below. The causes of the other types of upwelling are different but the actual upwelling is determined by the same process.

When a wind is blowing over the sea, the wind generates a current in the surface water. This surface current moves at an angle of 45° to the right of the wind (in the Northern Hemisphere) due to the Coriolis force.

The topmost water layer sets the underlying water in motion. At deeper levels the currents deviate further to the right and at the same time the strength diminishes. The net flow of the water current is perpendicular to the wind direction. This flow pattern is referred to as the Ekman spiral. (See fig. 2.1.) The flow of the water is called the Ekman transport and the layer, from the surface to where the flow of water is opposed to the wind direction, in which this process occurs is referred to as the Ekman layer.

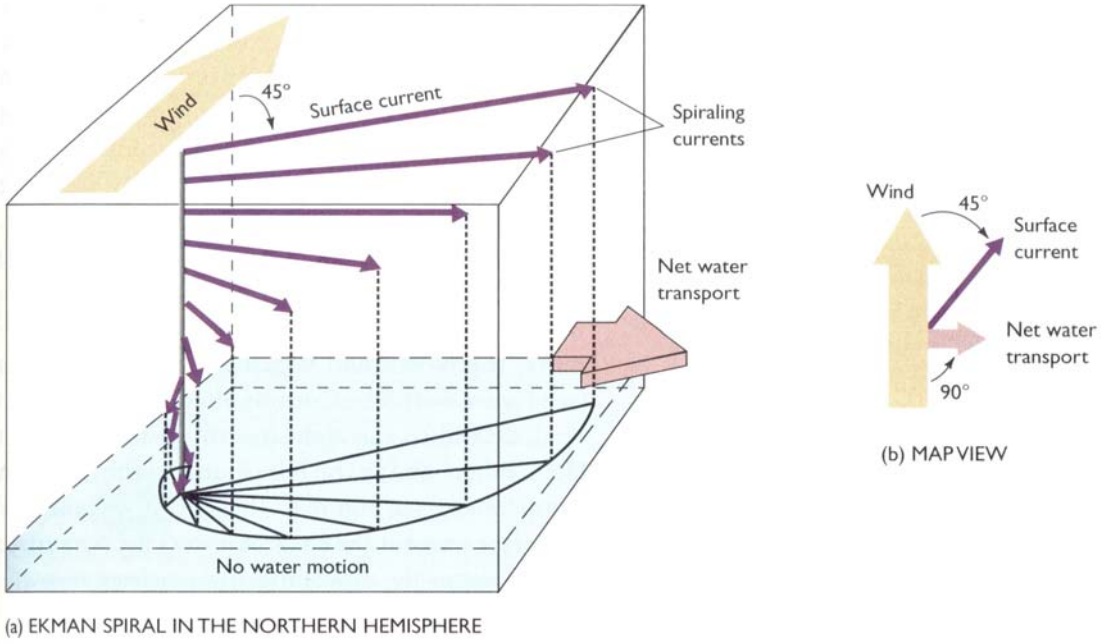

Figure 2.1 The Coriolis force causes a surface current 45° to the right of the direction of the generating wind. The surface water puts the underlying water in motion. As the current deepens each water layer is deflected slightly more to the right, producing a spiral pattern, the Ekman spiral. The net transport of water is perpendicular to the wind direction. (Figure from Pinet, 2003.)

Friction alone cannot be the only force responsible for the Ekman transport. If momentum was only transferred downwards by the friction between the molecules the Ekman layer would only be a fraction of its actual depth.

Frictional effects can be quantified through the molecular friction coefficient, λ_m, which is a measure of the viscosity of the fluid. If momentum is transferred downwards by molecular friction the depth of the frictional boundary layer (the distance over which the velocity is under the influence of the drag force of the wind) can be calculated from equation (2.1).

$$d = \sqrt{\frac{2\nu}{f}} \qquad (2.1)$$

Where d is the depth of the frictional boundary layer, ν is the kinematic molecular viscosity and f is the Coriolis parameter. Given that the kinematic molecular viscosity is in the order of 10^{-6} m/s^2 and the Coriolis parameter in the mid-latitudes is in the order of 10^{-4} s^{-1} the depth of the frictional boundary layer would be about 0.1 m.

The conclusion that can be drawn from this is that molecular friction alone cannot be responsible for the transfer of momentum. The transfer is achieved by turbulence. The water parcels moved by the turbulent eddies are several orders of magnitude larger than

the water molecules. The water parcels are much more efficient in exchanging their properties with the surroundings.

It is almost impossible to exactly describe every detail of the eddy field since it is chaotic by definition. Fluid dynamics has defined the coefficient of turbulent viscosity A_v (often referred to as the Austausch coefficient) that, for nearly all situations, can describe the effects of the eddy field. The associated boundary layer thickness is then given by equation (2.2).

$$d_E = \sqrt{\frac{2A_v}{f}} \qquad (2.2)$$

Typically the Austausch coefficient has a value of 0.1 m^2/s but can vary by an order of magnitude or more to either side. This will result in an Ekman layer that varies between 15 - 150 m.

When the wind is blowing parallel to the coast, with the coast to the left, the net flow of water will be directed away from the coast because of the Coriolis force and the resultant Ekman transport. To compensate for the seaward flow of water, colder and denser water from below is brought to the surface. This is the upwelling event. (See fig. 2.2.)

The deep-water has a higher salinity. The concentration of CO_2 is also larger than in the surface water because of the lower biological activity. Fewer of the phytoplankton can survive as the depth increases so the consumption rate of CO_2 diminishes. The higher amount of CO_2 in the deep-water is also due to the lower temperature which makes it possible for the water to solve more of the gas.

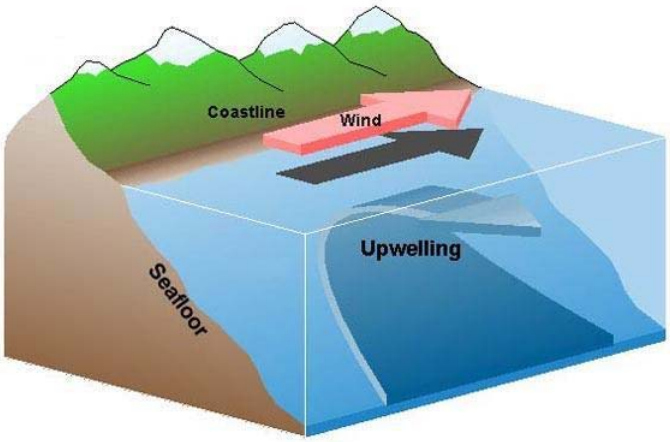

The upwelled water is also very rich in nutrients and is considered to be one of the major processes for nutrient regeneration in the surface layer.

Figure 2.2 A schematic picture of an upwelling. The wind is blowing parallel to the coastline and the Ekman transport creates a net flow of water to the right. To compensate for the seaward flow colder water must rise from below.
(Figure from http://oceanexplorer.noaa.gov/explorations/02quest/background/upwelling/media/fig1_cartoon.html, accessed on May 9, 2006)

2.2 Monin-Obukhov similarity theory

For a number of situations in the boundary layer the knowledge of the governing physics is insufficient to derive laws who describe what is observed. Observations in the boundary layer, however, often do show consistent and repeatable characteristics. Similarity theory is an empirical method of finding universal relationships between variables that are made dimensionless using appropriate scaling factors.

Monin-Obukhov theory is usually applied to the surface layer. The theory only works if the wind speed is not too low and u_* (the friction velocity) not zero. The surface layer is sometimes also referred to as the constant flux layer. Within the constant flux layer the fluxes should vary by less then 10% of their magnitude with height. Therefore one can simplify the description of the surface layer by using the measurements from just one height. Using the hypothesis that the fluxes are constant and having measurements from one height it is possible to use Monin-Obukhov theory to determine the fluxes, e.g. the sensible heat flux and fluxes of scalars such as water vapour and CO_2.

The following derivation of the Monin-Obukhov similarity theory is adapted from Högström and Smedman (1989).

The relevant parameters for the theory are the friction velocity u_*, the buoyancy parameter g/T, the scaling temperature T_*, the height z and the wind velocity gradient du/dz. The scaling temperature is defined according to equation (2.3) where $\overline{w'T_v'}$ is the virtual kinematic heat flux.

$$T_* = \frac{-\overline{w'T_v'}}{u_*} \qquad (2.3)$$

The first step of the derivation that will result in the Monin-Obukhov similarity theory is to perform dimensional analysis of the parameters of interest. First du/dz is made dimensionless with a combination of the other parameters. This is done according to equation (2.4).

$$\frac{du}{dz} \cdot z^a \cdot u_*^b \cdot T_*^c \cdot \frac{g^d}{T^d} = \text{dim. less} \qquad (2.4)$$

The values of the exponents a, b, c and d are derived from dimensional analysis, under the assumption that the stratification is neutral because otherwise it is not possible to find a unique solution to equation (2.4). This implies that T_* is zero, which makes the exponent c equal to zero as well. The dimensional analysis of the remaining part of equation (2.4) is expressed in equations (2.5) – (2.8).

$$t^{-1} \cdot l^a \cdot (l \cdot t)^b \cdot (l \cdot t^{-2} \cdot T^{-1})^d = 1 \qquad (2.5)$$

$$-1-b-2d=0$$
$$a+b+d=0 \qquad \text{(2.6-2.8)}$$
$$-d=0$$

Where t represents the dimension time, l the dimension length and T the dimension temperature. The result is that a = 1, b = -1 and d = 0. The resulting equation takes the form of equation (2.9). The von Karman's constant, k, can be added without violating the dimensional analysis since it has no dimension.

$$\frac{du}{dz}=\frac{u_*}{kz} \qquad (2.9)$$

Equation (2.9) can also be derived from differentiating the logarithmic wind profile.

For non-neutral conditions the expression can be written as in equation (2.10).

$$\frac{du}{dz}\cdot\frac{z}{u_*}=f(z,u_*,T_*,\frac{g}{T})=h(\zeta)=\text{dim. less} \qquad (2.10)$$

That is, the dimensionless velocity profile is a function of height, friction velocity, the scaling temperature and the buoyancy parameter which also is a function h(ζ). Where ζ is a dimensionless combination of the parameters z, u_*, g/T and T_*. Dimensional analysis results in equations (2.11) – (2.15).

$$z^{\alpha}\cdot u_*^{\beta}\cdot T_*^{\gamma}\frac{g^{\delta}}{T^{\delta}}=\zeta \qquad (2.11)$$
$$l^{\alpha}\cdot(l\cdot t^{-1})^{\beta}\cdot T^{\gamma}\cdot(l\cdot t^{-2}\cdot T^{-1})^{\delta}=1 \qquad (2.12)$$

$$\alpha+\beta+\delta=0$$
$$-\beta-2\delta=0 \qquad \text{(2.13-2.15)}$$
$$\gamma-\delta=0$$

The solution to equations (2.13) – (2.15) is that α = γ = δ and β = -2δ. This gives ζ the solution (2.16).

$$\zeta=\left(\frac{zT_*g}{u_*^2T}\right)^{\delta} \qquad (2.16)$$

The shape of the function h(ζ) is not known so it is possible to multiply the expression with von Karman's constant and insert the definition of T_* from equation (2.3). The result is equation (2.17).

$$\zeta = \frac{z}{-\frac{u_*^3 \cdot T}{g \cdot k \cdot \overline{w'T_v'}}} = \frac{z}{L} \qquad (2.17)$$

L is the Monin-Obukhov length and z/L is a measure of the stability. When the stratification is neutral z/L equals zero. During stable conditions z/L is positive and during unstable conditions it is negative.

The reason why this parameter is defined is that gradients (e.g. the horizontal wind gradient as in the derivation above) of interest in the boundary layer can, if they are made dimensionless correctly, be expressed as unambiguous functions of z/L. The shape of the function must be identified by direct measurements. When this shape is known the Monin-Obukhov similarity theory can be used to estimate the turbulent fluxes.

2.3 Spectra

A spectrum is a way of illustrating the distribution of energy relative to the wavelength or the frequency. In meteorology spectral analysis is mostly used to illustrate the turbulent energy as a function of the frequency. The turbulent energy in the atmosphere is carried by eddies of different sizes. Measurements usually take place at only one point. Thus one must assume that the eddies are advected past the measuring site with the mean wind (Taylor's hypothesis). The measurements gives the frequency of the flux and applying Taylor's hypothesis gives the size (i.e. the diameter) of the eddies. Thus the high frequency eddies are smaller and the low frequency eddies are larger.

The autocorrelation of the variance of a parameter, say u, can be calculated and then rewritten using Fourier's integral theorem. The conditions that restrict the use of this theorem are very generous. This means that a random process that is a function of time, such as turbulence, can be described by a Fourier integral.

Suppose that u varies randomly as time progresses. The autocorrelation of u can also be expressed as a Fourier integral, equation (2.18,) where ρ(t) is the autocorrelation function.

$$\overline{u^2}\rho(t) = \int_{-\infty}^{+\infty} e^{i\omega t} \cdot \Phi(\omega) d\omega \qquad (2.18)$$

If u is a component of the velocity then $\overline{u^2}$ is the double energy of the velocity component u. This means that Φ(ω) is an energy spectrum.

The inverse function of the Fourier expression of autocorrelation, or in shorter terms equation (2.18), is resulting in equation (2.19).

$$\Phi(\omega) = \frac{1}{2\pi} \int_{-\infty}^{+\infty} e^{-i\omega t} \cdot \overline{u^2} \cdot \rho(t) dt \qquad (2.19)$$

An autocorrelation function always gives the same result regardless if the difference in time is positive or negative as long as it is of equal length. Thus ρ(t) is an even function of t. Also Φ(ω) is an even function. This can be proved by substituting t with –t in equation (2.19). Such substitution is not shown here but it gives two further characteristics of Φ(ω). The function is always real and positive. This implies that equation (2.19) can be simplified into equation (2.20)

$$\Phi(\omega) = \frac{1}{\pi} \int_{0}^{\infty} \overline{u^2} \cdot \rho(t) \cdot \cos(\omega t) dt \qquad (2.20)$$

The size of the energy-containing eddies in the atmosphere usually vary greatly in size, over several orders of magnitude. Because of this the spectra are more easily studied if the x-axis shows the logarithm of the frequency.

2.4 Co-spectra

A spectrum can also be used to study the fluctuations of two parameters. If the time series of the fluctuations of, e.g. w'(t) and θ'(t) are known it is possible to create a new time series w'θ'(t) and perform spectral analysis on it.

From this a number of different types of spectra can be obtained using Fourier transforms. From the real part of the cross spectrum the co-spectrum is obtained. The co-spectrum is frequently used in meteorology because the sum of all co-spectral amplitudes equals the covariance of the parameters for which the co-spectra was calculated. Also the integration over all frequencies of the co-spectra gives the total flux.

The co-spectra of w and θ can be used to study the flux of sensible heat and also the stability. If the integral area of the co-spectra is positive the stratification is unstable and if it is negative the stratification is stable.

2.5 Bulk calculations

The vertical flux of any variable is assumed to be driven by the difference of the variable in question across the interface. The flux is also dependent on the transport velocity. This velocity is usually parameterized as a function of some measure of turbulence.

According to the bulk transfer law the relationship between surface kinematic flux and any meteorological variable is proportional to the wind speed and the difference of the variable in question between the surface and some reference height, usually 10 m above the surface. In order to correctly describe the fluxes a correctional coefficient must also be added, the bulk transfer coefficient, which represent other processes of importance.

There are several bulk transfer coefficients. The most common are the coefficient for momentum transfer, also known as drag coefficient, and the coefficients for heat and moisture, the former also referred to as the Stanton number and the latter as the Dalton number. The value of the coefficients must be determined empirically.

The values of the bulk transfer coefficients are heavily dependent on the stability. Unstable flows cause a greater flux than stable. Because of this the bulk transfer coefficients are modified using a stability-dependent correction term.

The surface roughness also play a part in determining the bulk transfer coefficients. The rougher the surface is the more likely it is to cause more intense turbulence. Over oceans the surface roughness is associated with ocean wave height, a known function of surface stress or wind speed.

The sensible heat flux is determined by the difference in temperature between the atmosphere at 10 m above the surface and the temperature of the air just above the water surface, which is estimated to be equal to the SST. The heat exchange is also dependent on the wind speed at 10 m. Equation (2.21) shows the formula that is used.

$$H = \rho \cdot c_p \cdot C_H \cdot u \cdot (T_{water} - T_{air}) \qquad (2.21)$$

Where H is the latent heat flux in W/m^2 and ρ is the density of the air, u is the wind speed at 10 m and C_H is the bulk transfer coefficient for sensible heat.

The latent heat flux, E, is estimated by equation (2.22) which clearly shows that the latent heat flux is dependent on the difference between the saturation level of moisture for the atmosphere at 10 m, q_s, and the actual amount of moisture in the atmosphere, q, at the same level.

$$E = \rho \cdot L_V \cdot C_E \cdot u \cdot (q_s - q) \qquad (2.22)$$

L_V is the latent heat of vaporization and C_E is the bulk transfer coefficient for latent heat.

The bulk transfer coefficients C_E and C_H in this study are adapted from Rutgersson et al. (2001). They are both assumed to have a neutral value of 1.1×10^{-3}. The neutral values of the bulk transfer coefficients are then modified using stability corrections.

The bulk calculation of the CO_2-flux is described in equation (2.23). The bulk flux is dependent on the CO_2-gradient and wind speed, but also on the solubility of CO_2, K_0, in the water which is temperature dependent. The solubility is also dependent on the salinity of the water, but this investigation does not include measurements of the salinity so the salinity is assumed to be constant. This formula is adapted from Wanninkhof (1992).

$$F = K_0 \cdot k \cdot (CO_{2sea} - CO_{2atmosphere}) \qquad (2.23)$$

The transfer velocity, k, is defined in equation (2.24).

$$k = 0.31 \cdot u^2 \cdot \sqrt{\frac{660}{Sc}} \qquad (2.24)$$

Sc, the Schmidt number, is proportional to the viscosity divided by the molecular diffusivity and is also dependent on the temperature.

2.6 Eddy correlation method

The fluxes of scalars can be measured directly using the eddy correlation method. Fast-response instruments generate time series of state variables. From these time series the perturbation values of the data points are calculated. Multiplying the respective perturbation time series gives the kinematic turbulent flux, e.g. w'θ'(t).

When the time series of the perturbations are calculated simple multiplication and averaging (Reynold's averaging) can give the kinematic fluxes, the variance, turbulent kinetic energy, fluxes of variances (e.g. $\overline{w'^2\,\theta'}$), fluxes of energies and higher moments.

The advantage of this method is that it is direct and it is simple. A disadvantage is the fast-response sensors that must be used should be able to measure using a frequency of 10-20 Hz. These sensors are quite expensive. Another disadvantage is that the measurement errors in the original time series compound themselves as higher and higher moments are calculated. By the third or fourth moment the error (noise) is as large or even larger than the signal.

2.7 The Webb correction

When applying Reynold's averaging to a vertical flux it is divided into two components: the turbulent flux and the mean transport. The mean transport can, usually, be neglected for continuity reasons and the turbulent flux is considered to be representative of the total flux.

This simplification does not hold generally because turbulent motion is made up of ascending and descending air parcels which have different densities. The former being the less dense parcels and, consequently, the latter are denser. Because the mass balance must be obtained the vertical velocity of the ascending parcels must be different from that of the descending ones. This implies that the mean vertical velocity is not zero. Thus the turbulent flux obtained from the eddy covariance measurements has to be corrected to give the total constituent flux. This is called the Webb correction.

Different approaches to the Webb correction parameterise the mean vertical velocity in different ways. The mean concentration of the constituent is always obtained from measurements.

The significance of the Webb correction dependence on which flux it is applied to. The correction for water vapour (latent heat) is 2-3 % but for CO_2 the Webb correction is 20-30 % of the flux, (Liebethal and Foken, 2003).

3 Method

3.1 Measuring site

The measurements in this investigation are taken at the Östergarnsholm-site, east of Gotland in the Baltic Sea during the summer of 2005. Östergarnsholm is a low flat island without any trees. At the southernmost tip of the 1 km long peninsula in the south-eastern part of the island a 30 m tower has been erected. If the wind is blowing from the sector 80° – 220° (E to SW) the fetch area is representative of the marine air, since the wind is blowing from the sea. Figure 3.1 shows the Östergarnsholm-site and its surroundings. The location of the measuring buoys and the ship Aranda mentioned below are also shown.

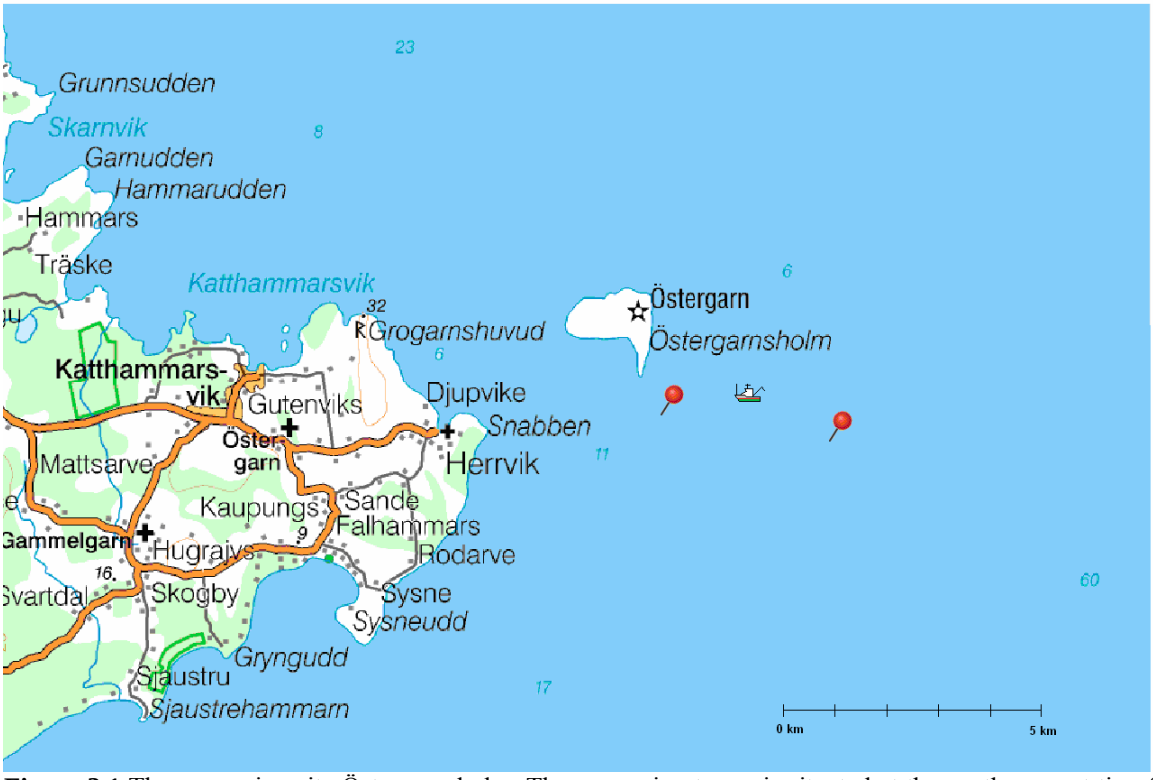

Figure 3.1 The measuring site Östergarnsholm. The measuring tower is situated at the southernmost tip of the island. The pin closest to the tower shows the location of the CO_2-buoy. The little ship shows were Aranda was anchored Aug 29. The second pin, farthest away from the tower, represents the location of the wave rider-buoy used by Smedman et al. (1999).

The buoy to the right in fig. 3.1 (represented by a pin) is the wave rider buoy used by Smedman et al. (1999). The buoy is moored 4 km southeast of the tower and the wave field there is considered to be representative of wave field in the footprint area.

The footprint area is the area at some distance upwind from the tower where the turbulent fluxes that the tower measures originate from. The location of the footprint area is dependent on the wind and the stratification.

The tower is instrumented with slow-response sensors designed at the Department of Meteorology, Uppsala University, which measures temperature, wind speed and direction at the heights: 7, 11.5, 14, 20 and 28 m. Turbulent fluctuations are recorded with SOLENT 1012R2 sonic anemometers at the heights: 9, 17 and 25 m. Humidity fluctuations are only measured at the lowest level. The CO_2-measurements are performed by a LICOR-7500 at the 9 m-level. The measurements are taken with a sampling frequency of 1 Hz for the slow-response (profile) sensors and 20 Hz for the turbulence signals.

The data, both the profile and the turbulence data, are one hour averages. To eliminate possible trends, a high pass filter based on a 10 min running average is applied to the turbulence time series prior to calculating variances and covariances.

The measurements in the water comes from a buoy moored about 1 km south-southeast of the tower. It has a SAMI sensor that measures the pH and the alkalinity of the water using photospectrometric methods. From these parameters the pCO_2 is calculated. The buoy measures CO_2 and the SST 5 m below the surface. Data from the sea during Aug 29 comes from the ship Aranda of the Finnish Institute of Marine Research.

3.2 Identifying and analysing the upwelling situations

The definition of an upwelling event in this study is that the SST must drop at least 4°C in 5 hours. At the same time there must be a simultaneous increase in the amount of CO_2 in the surface water by at least 20 ppm. Data were also required to have a wind direction between 80° and 220° so that the wind was blowing from the sea.

Stability was studied with respect to z/L, the temperature difference between SST and the atmospheric temperature at 10m ($\Delta T=T_{air}$-SST), temperature profiles and the co-spectra of w' and T'.

The turbulent fluxes that are studied are the kinematic fluxes of sensible and latent heat and of CO_2. These are obtained from eddy correlation method and the Webb correction was applied to the flux of CO_2. These values are compared to the bulk calculation of the same fluxes.

4 Results

Four situations of distinct upwelling, which satisfied the demands were found: June 24, July 12, July 15 and August 29. Only the measurements taken from the upwelling situation on July 15 can be used during the entire upwelling event. The wind does not change direction until the SST is back to the approximately the value it had before the upwelling event started. During the other three cases, August 29, July 12 and June 24, the wind changes direction when the SST is approaching its lowest value. After this the measurements can no longer be considered to be representative of the marine air since the wind is blowing over too much land.

4.1 Description of the fluxes

4.1.1 June 24

The first upwelling event this summer that fulfils the requirements starts in the afternoon of June 24. (See fig. 4.1.) The SST falls from ~15°C to below 11°C six hours later. As the SST drops 4°C the CO_2 level increase with 20 ppm. When the SST is at its lowest value the wind speed abruptly decreases, from 10 m/s to 2 m/s at the same time as the wind also changes direction from south-southwest to west.

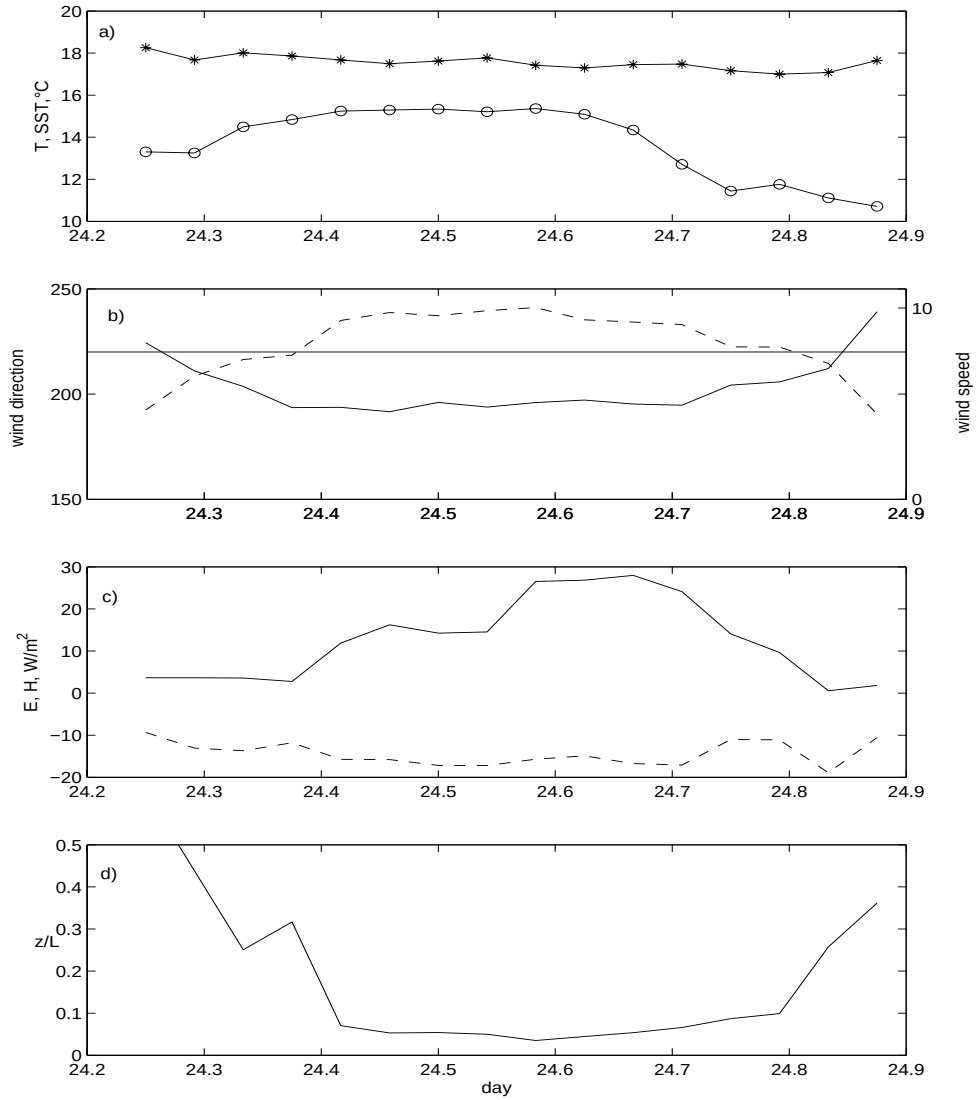

Figure 4.1 Measurements from June 24 of a) SST (circles) and air temperature (stars), b) wind direction (solid line) and wind speed (dashed line), the thin solid line represents the limit of undisturbed wind direction, c) latent heat (solid line) and sensible heat (dashed line) and d) z/L.

4.1.1.1 Stability and heat fluxes

The air temperature remains higher than the SST during the entire day. This indicates that the atmosphere should have a stable stratification. The stratification is stable all the time but as the upwelling starts the stratification becomes more stable. This can is seen both in z/L and the temperature profiles, (see appendix B, fig. B1).

The co-spectra of w'T' (shown in fig. 4.2) are showing a negative flux and thus indicate a stable stratification. The most stable value is not at the time of the smallest SST-value. This is probably due to the very low wind speed at the time of the lowest SST.

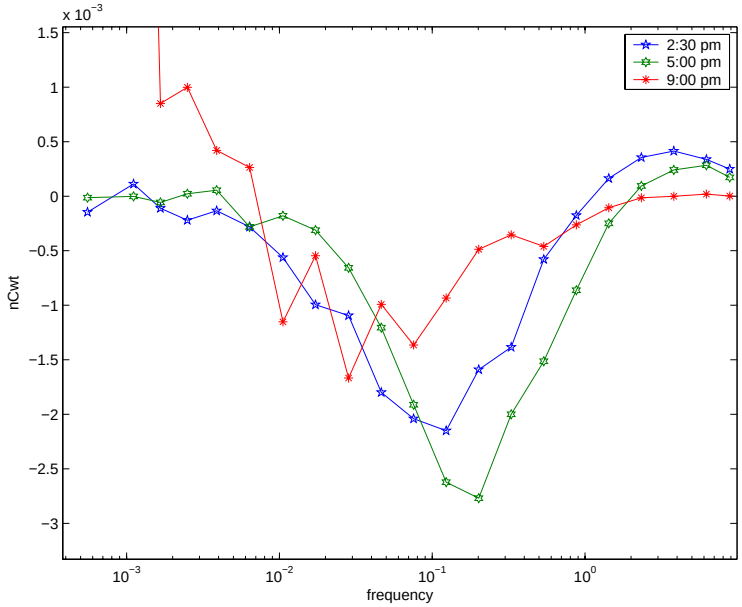

Figure 4.2 The co-spectra of w'T' on June 24.

The sensible and the latent heat fluxes are shown in fig. 4.3. The bulk calculations thereof using equations (2.21) and (2.22) are also shown in the same figure.

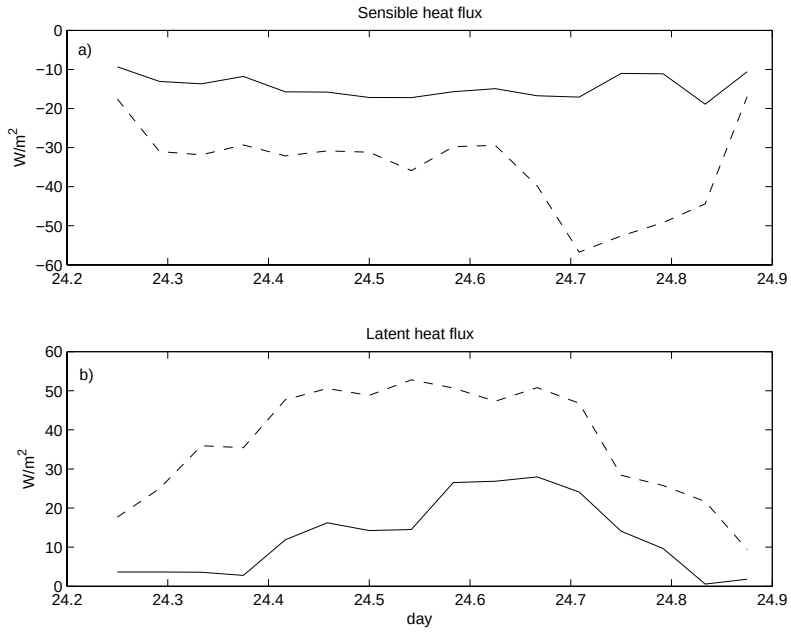

Figure 4.3 a) The sensible heat flux (solid line) and the bulk calculation (dashed line) of this flux.
b) The latent heat flux (solid line) and the bulk calculation (dashed line) of the flux.

The sensible heat flux is directed from the atmosphere to the sea. No change in direction can be observed from a time series and the change in the size of the flux is small. The bulk calculation gives a stronger negative flux before the upwelling event but as the upwelling starts the bulk calculation gives a the flux that is twice as large as the

measurements. When the SST reaches its lowest value the bulk calculation is almost as small as the measurements.

The latent heat flux decreases at the same time as the SST decreases. This decrease is perhaps more due to the fact that the wind speed also decreases. The bulk calculation shows the same trend as the measurements but overestimates the flux.

4.1.1.2 Flux of CO_2

Even though the level of CO_2 is higher in the atmosphere than in the ocean the measurements show a positive flux. (See fig. 4.4.) The flux measurements show a positive (counter-gradient) but decreasing flux of CO_2. The reason for the counter-gradient flow is not obvious because the wind speed is relatively large so both the atmosphere and the sea should be well mixed.

The bulk calculation (not shown here) shows a much larger flux that is negative and decreases as the upwelling progresses. When the SST is at its lowest value the bulk calculated flux is almost zero.

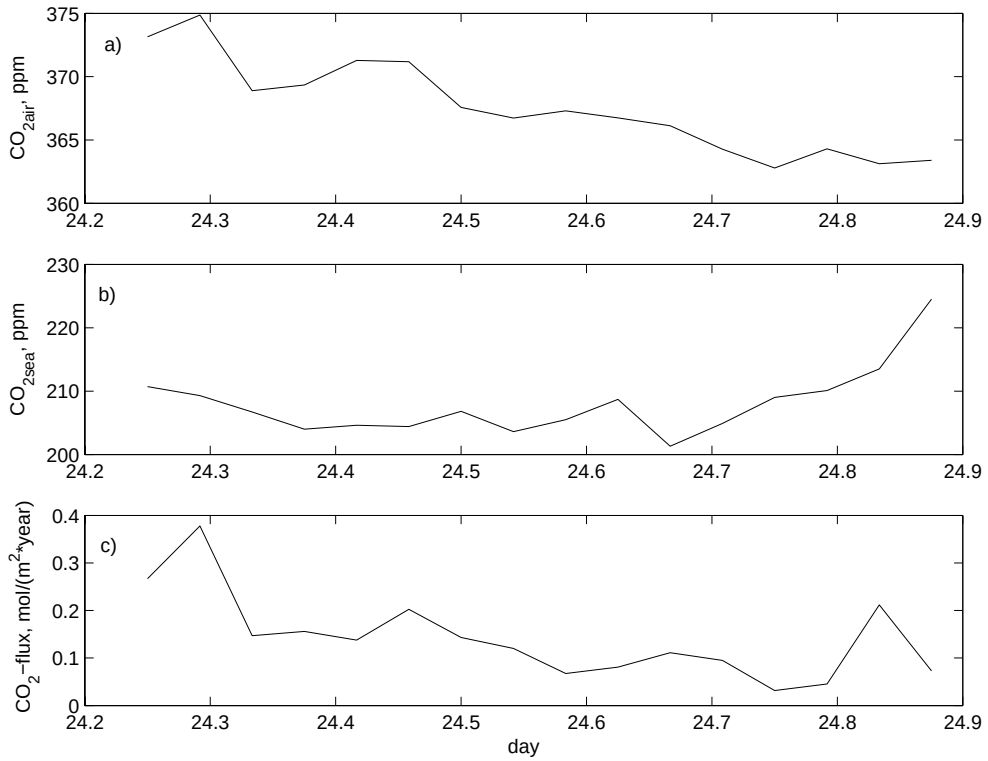

Figure 4.4 The CO_2 measurements from June 24, a) the concentration of CO_2 in the air, b) the concentration of CO_2 in the sea and c) the flux of CO_2.

The spectra and co-spectra of CO_2 are shown in fig. 4.5. Both spectra and co-spectra show an initial increase and show a rapid decrease with the last spectrum at 9 pm. This decrease is, as is the case for the co-spectra of w'T', most likely a result of the low wind speed. This indicate that the turbulent fluctuations, and thus the flux, is very small and the spectra mostly show the mesoscale variations in the fluctuations.

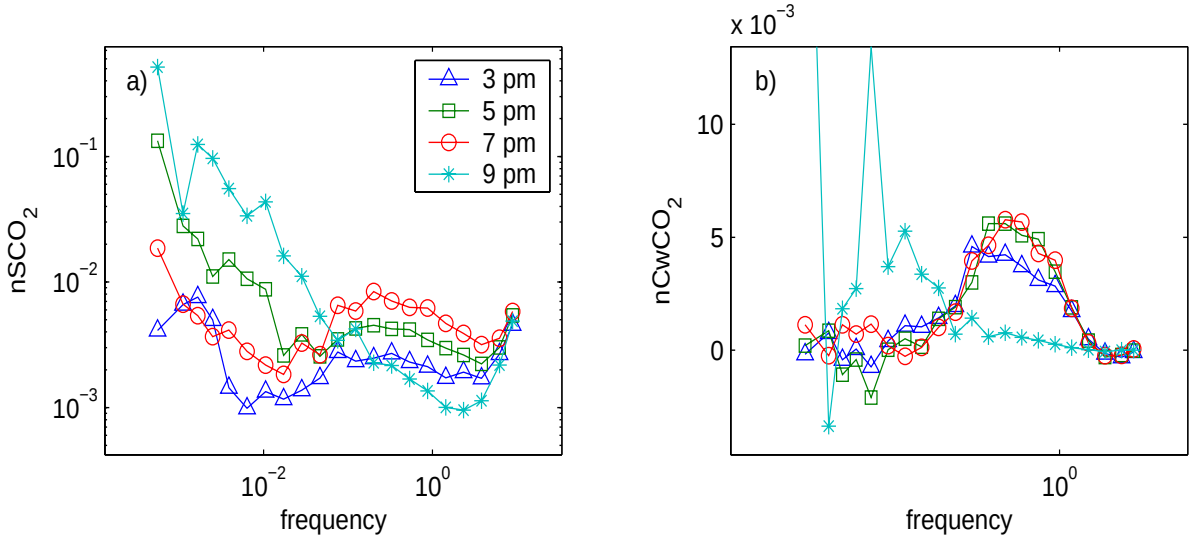

Figure 4.5 a) The energy spectra and b) the co-spectra of CO_2 on June 24.

4.1.2 July 12

The wind is once again coming from south-southwest, along the coast of Gotland, and causes an upwelling event. The SST increases during from the morning on July 12 till the afternoon (2:30 pm), then the increasing trend stops and the SST decreases. (See fig. 4.6.) At the same time as the SST decreases the CO_2-levels in the water increases from 140 ppm to 190 ppm.

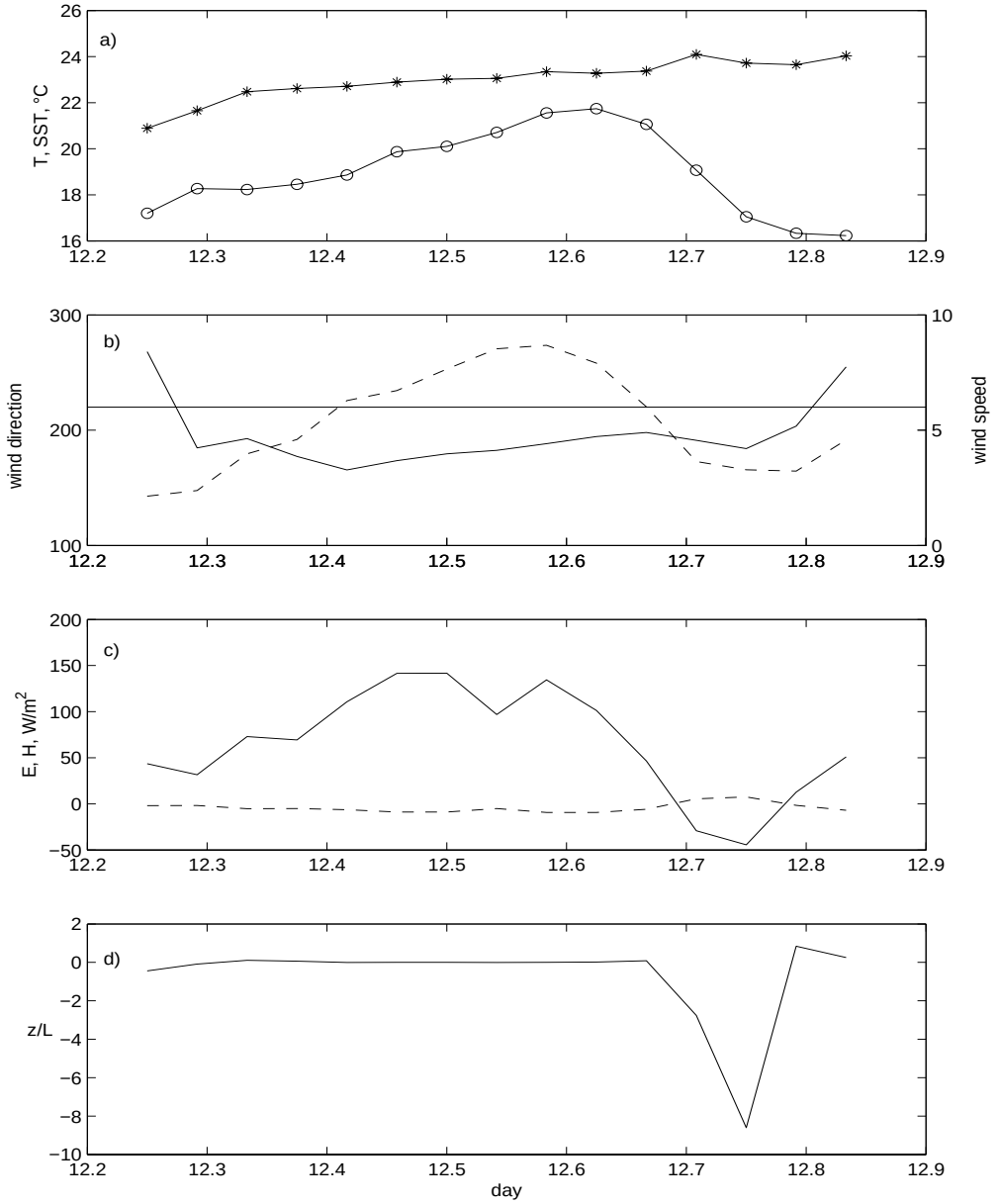

Figure 4.6 Measurements from July 12 of a) SST (circles) and air temperature (stars), b) wind direction (solid line) and wind speed (dashed line), the thin solid line represents the limit of undisturbed wind direction, c) latent heat (solid line) and sensible heat (dashed line) and d) z/L.

4.1.2.1 Stability and heat fluxes

The air temperature is higher relative the SST throughout this day. This is an indication of a stable stratification, but z/L is behaving rather peculiar. It is slightly negative before the upwelling event and has a sudden inexplicable drop during the middle of the upwelling event.

The co-spectra of w' and T' indicate an unstable stratification before the upwelling, which later stabilizes and becomes stable as the SST is approaching its lowest value. (See fig. 4.7.)

Nothing unexpected can be seen in the temperature profiles from this day. They show an atmosphere that is slightly stable or neutral that becomes more and more stable as the SST decreases. (See appendix B, fig. B2.)

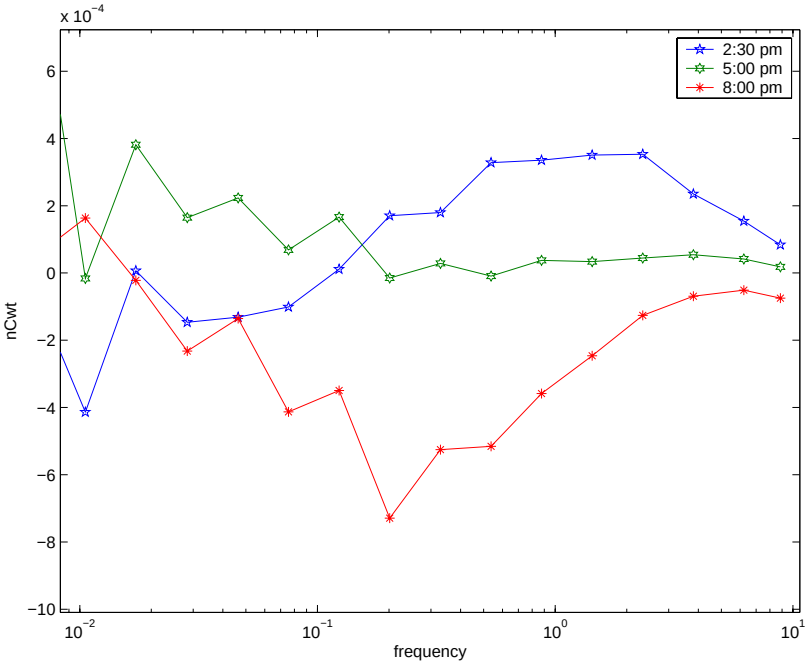

Figure 4.7 The co-spectra of w'T' on July 12.

The sensible heat flux (see fig 4.8a) is negative before the upwelling event because the atmosphere is warmer than the sea. As the upwelling starts the temperature difference increases and the sensible heat flux should increase negatively. Having this in mind it is strange that the observations shows that the flux diminishes and becomes positive. The bulk calculation remain negative throughout this period but it also shows a decrease in the flux as the SST decreases. The decrease, both of the measured and the calculated flux, is most likely due to the decreasing wind speed.

The latent heat flux (see fig. 4.8b) is showing a similar trend as the wind speed and the SST. As the wind and the SST increase the latent heat flux increase. When the upwelling event starts both wind speed and SST decrease as well as the latent heat flux, although the minimum in the latent heat flux occurs before the lowest value of the SST. The bulk calculations follows the same trend as the measurements.

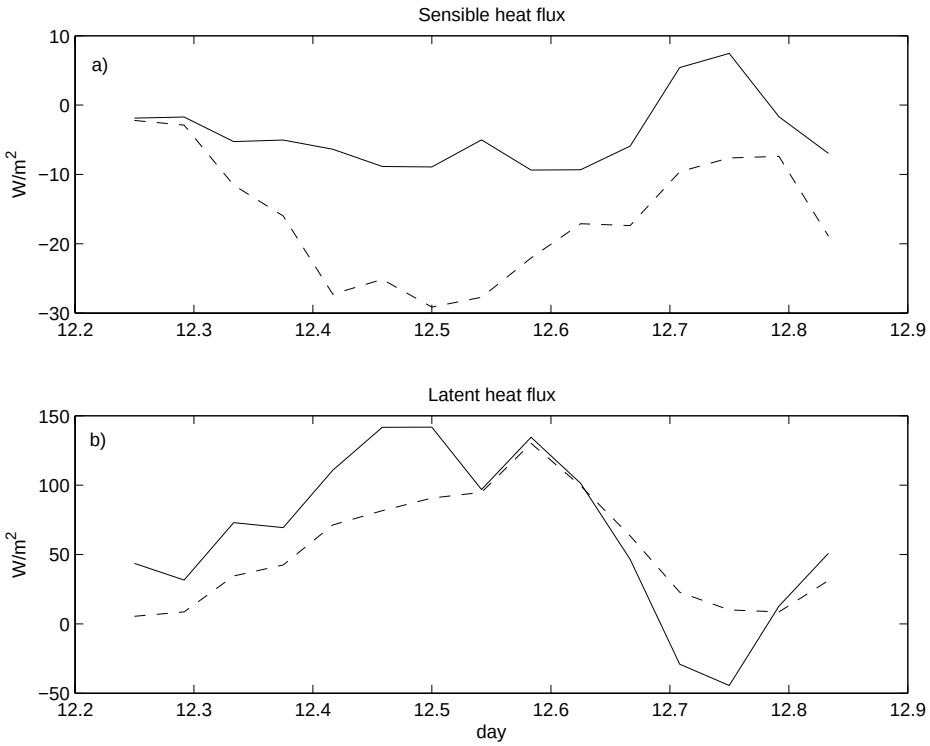

Figure 4.8 The SST and the heat fluxes on July 12. The solid lines represent the measurements and the dashed lines the bulk calculations.

4.1.2.2 Flux of CO_2

As the upwelling event starts the flux of CO_2 decreases. (See figure 4.9.) The flux is negative (i.e. directed downwards) but as the upwelling event reaches its maxima the flux changes direction. The bulk calculation never becomes positive but shows the same trend as the measurements. However, the bulk-calculated flux is approximately 30 times larger than the measurements and thus not included in the figure.

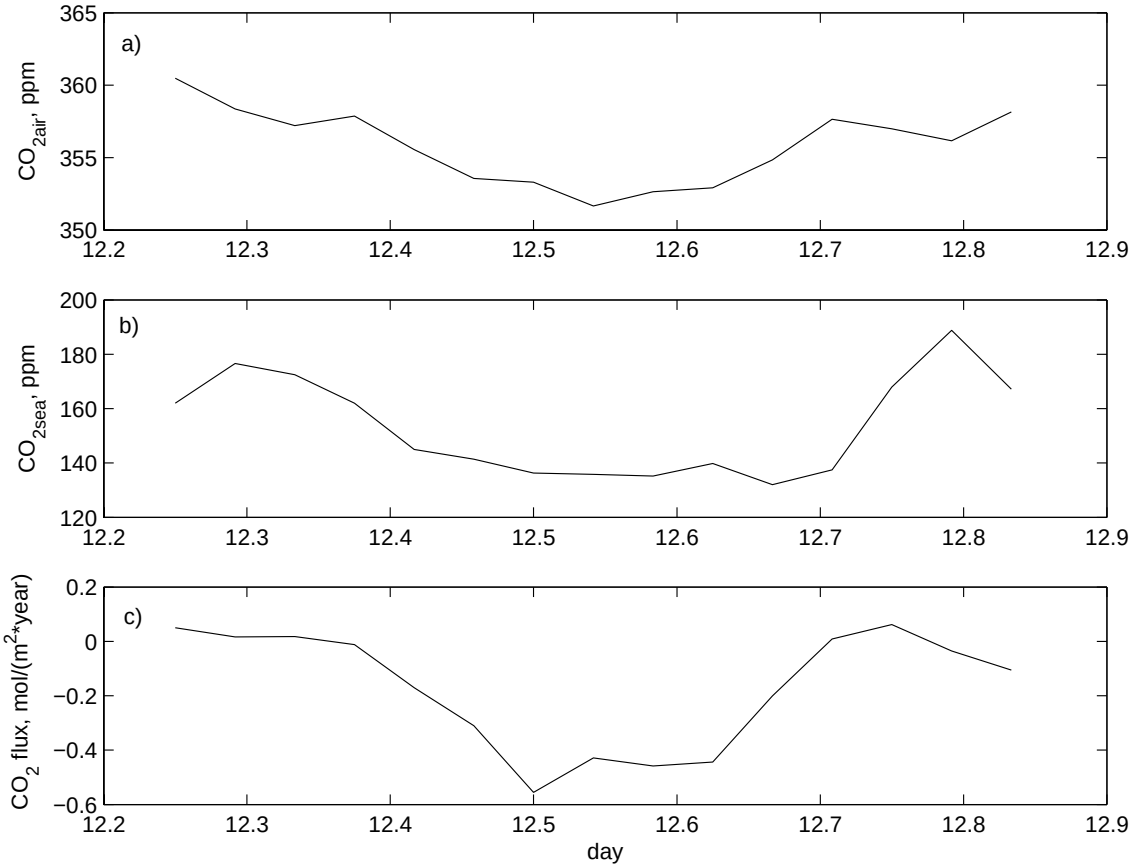

Figure 4.9 The CO_2 measurements from July 12, a) the concentration of CO_2 in the air, b) the concentration of CO_2 in the sea and c) the flux of CO_2.

The change in direction of the flux is not observed in the co-spectra that are shown here, but they do show that the flux decreases as the upwelling starts. The spectra also show a decrease in the energy of the CO_2-fluctuations. (See fig. 4.10.)

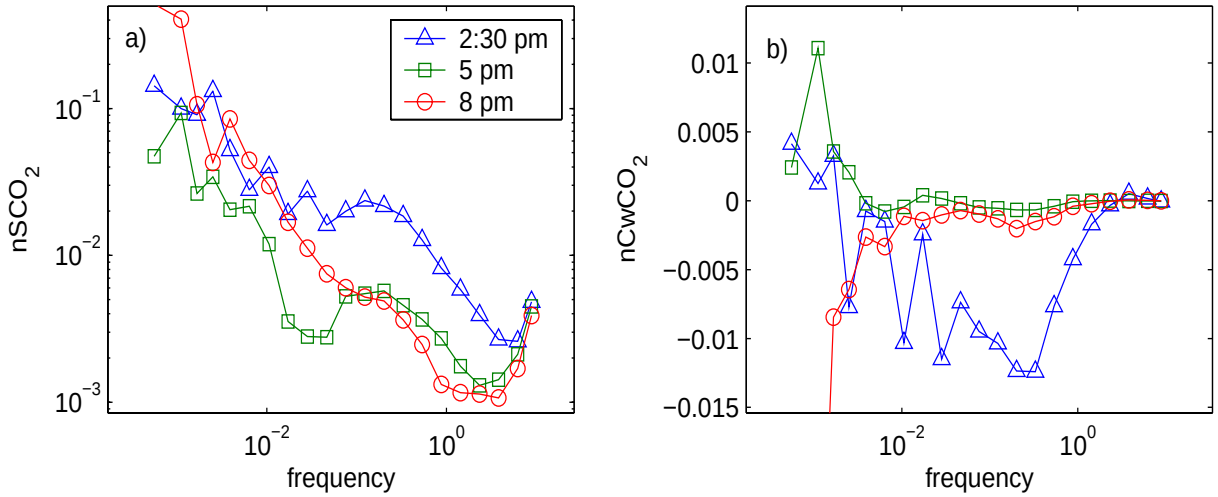

Figure 4.10 a) The energy spectra and b) the co-spectra of CO_2 on July 12.

4.1.3 July 15

This is the only upwelling situation in the available data where the wind doesn't change direction to above 220° before the SST reaches its lowest value. The upwelling event starts at 2:30 pm and is over by midnight, when the SST is back to higher degrees again. (See figure 4.11.) The CO_2-level is ~130 ppm before the upwelling. When the SST is at its lowest value the CO_2-level has a peak value of 206 ppm.

Before and during the upwelling event the wind speed is approximately 10 m/s and the wind direction changes from 200° to 150°. When the SST increases the wind becomes more westerly (above 220°) and the wind speed decreases.

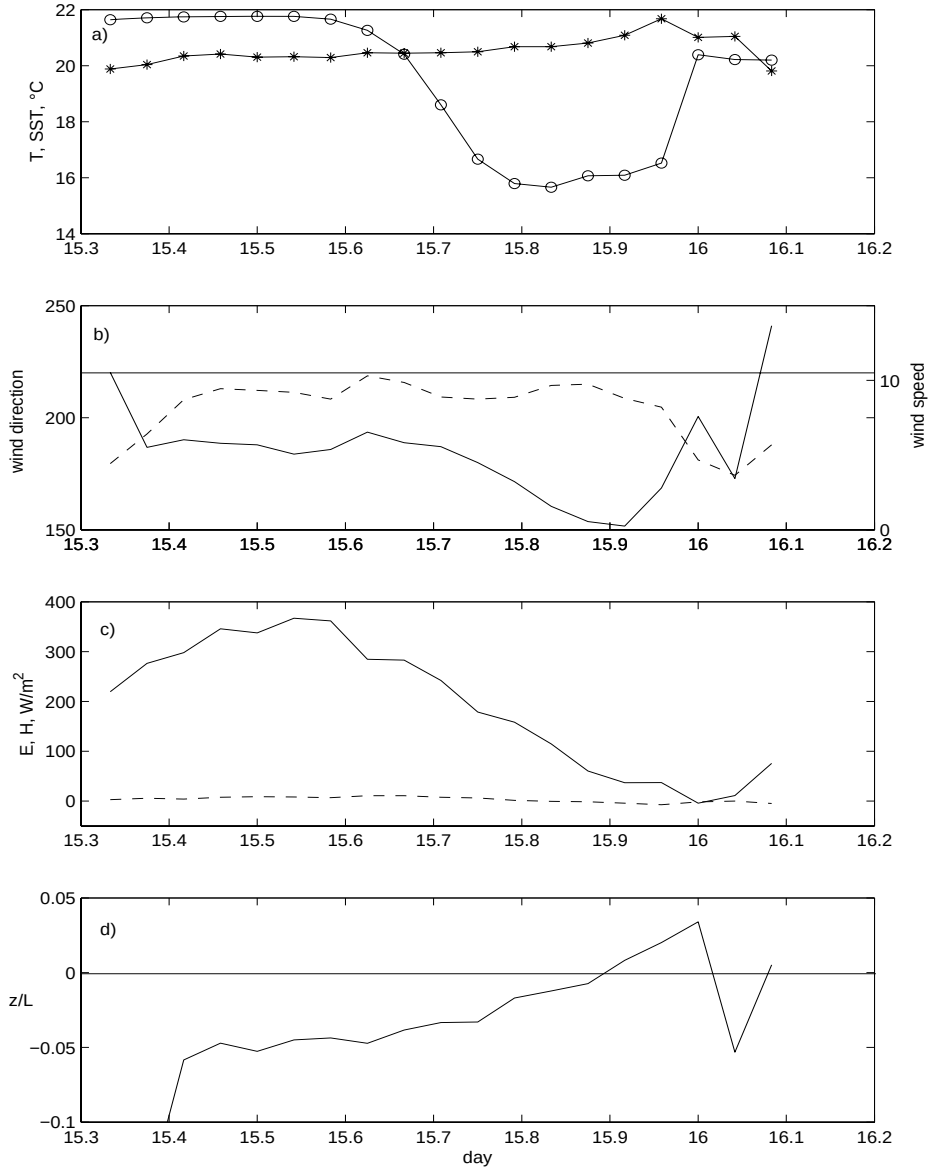

Figure 4.11 Measurements from July 15 of a) SST (circles) and air temperature (stars), b) wind direction (solid line) and wind speed (dashed line), the thin solid line represents the limit of undisturbed wind direction, c) latent heat (solid line) and sensible heat (dashed line) and d) z/L.

4.1.3.1 Stability and heat fluxes

The different ways of determing the stability are not entirely conclusive for this upwelling event. (See figures 4.11a, d and 4.12.) The difference between SST and air temperature (fig. 4.11a) indicates that the stratification becomes stable at 4:00 pm, when the upwelling has just started, but z/L (fig. 4.11d) does not become stable till 9:00 pm, when the upwelling already has reached its maximum. The co-spectra of w' and T' (fig. 4.12) show a decrease in the fluctuations of w'T' and thus a stabilization during the latter half of July 15. The stratification is not becoming stable until midnight, after the entire upwelling event is over and the SST is back to its normal level.

The temperature profile (see appendix B, fig. B3) shows a similar behaviour as the co-spectra and z/L, an unstable stratification that stabilizes as the SST decreases. According to the temperature profiles the atmosphere does not have a stable stratification until the SST is back to its normal values.

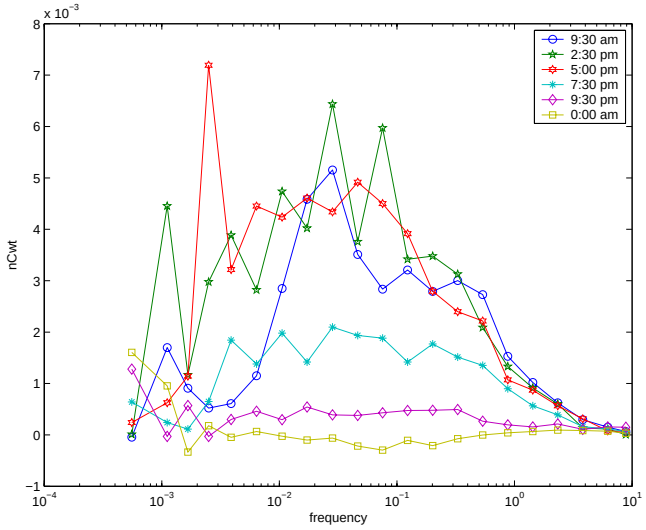

Figure 4.12 The co-spectra of w'T' on July 15.

The sensible flux is decreasing as the upwelling progresses. The behaviour of this flux and the bulk calculation thereof are discussed in more detail in section 4.3.

Before the upwelling event the latent heat flux is increasing, probably due to the fact that the wind speed also is increasing at the same time. As the upwelling starts the latent heat flux decreases. The wind speed is now more or less constant. The bulk calculation (not shown) underestimates the flux both before and during the upwelling event, but as the SST rises the calculated flux shows a better agreement with the measurements.

The spectra of q' show that the energy of the flux is decreasing. The energy is steadily decreasing, both when the SST decreases and when the SST increases again. (See fig 4.13.)

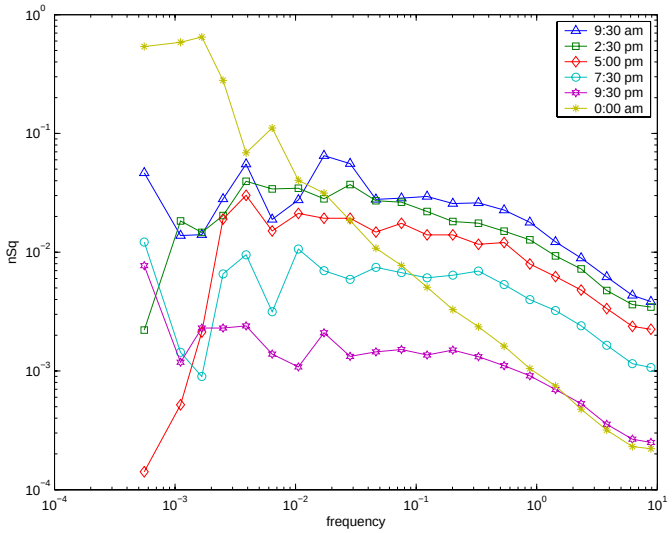

Figure 4.13 The energy spectra of q' on July 15.

4.1.3.2 Flux of CO_2

Before the upwelling event the flux of CO_2 is increasing. When the upwelling starts the trend of the flux changes and it approaches zero. (See fig. 4.14.) The bulk calculated flux (shown in fig 4.29) also shows the same trend but once again it is much larger than the measurements.

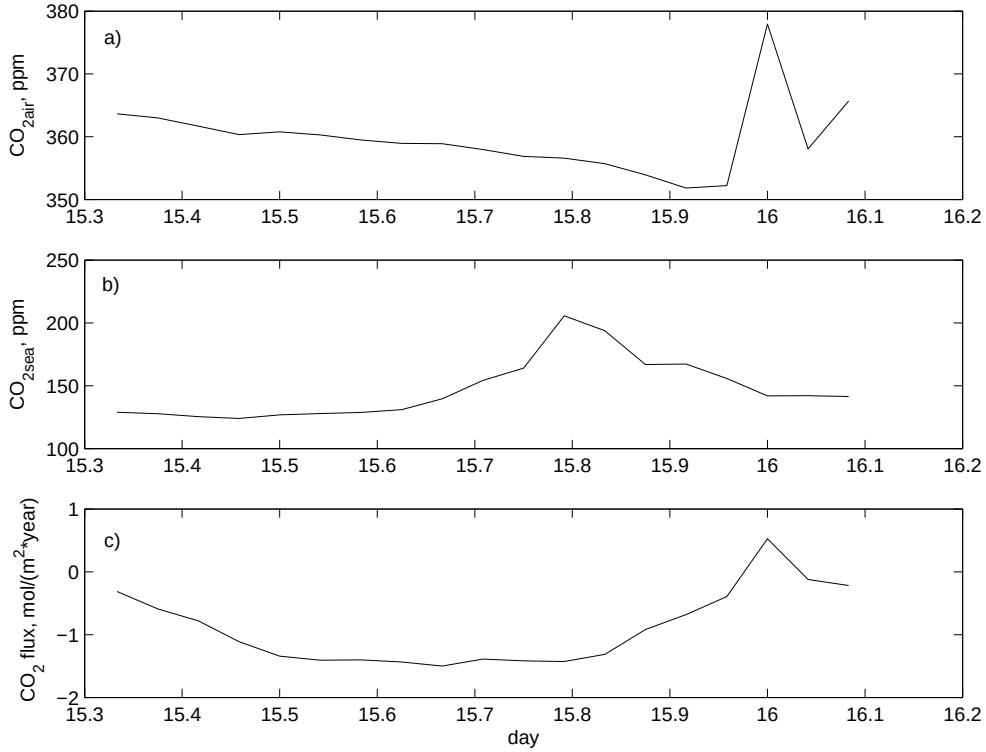

Figure 4.14 The CO_2 measurements from July 15, a) the concentration of CO_2 in the air, b) the concentration of CO_2 in the sea and c) the flux of CO_2.

The co-spectra of w' and CO_2' and the energy spectra of the CO_2-fluctuations both show a decrease in the flux. (See fig 4.15.)

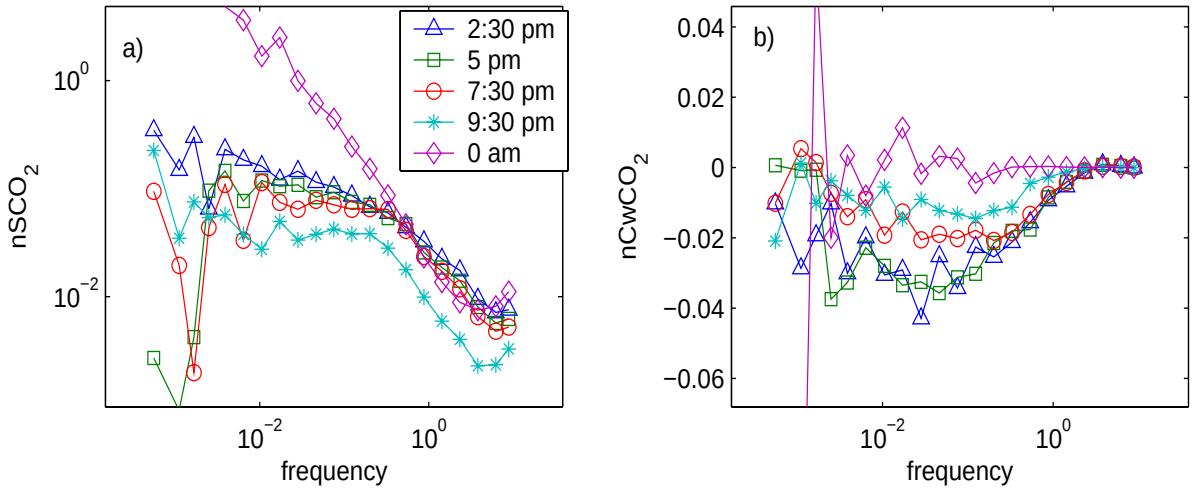

Figure 4.15 a) The energy spectra and b) the co-spectra of CO_2 on July 15.

4.1.4 August 29

The upwelling event starts at 7:00 pm when the wind has been blowing from south-southwest for most of the day (around 200°, i.e. along the coast of Gotland). The SST was close to 16°C prior to the upwelling event. The last measurement of SST, before the wind turns and reaches a direction of more than 220°, is slightly above 11°C. This means that the SST decreases 5 degrees. (See fig. 4.16.) Simultaneously the amount of CO_2 in the water rises from ~300 ppm to 450 ppm.

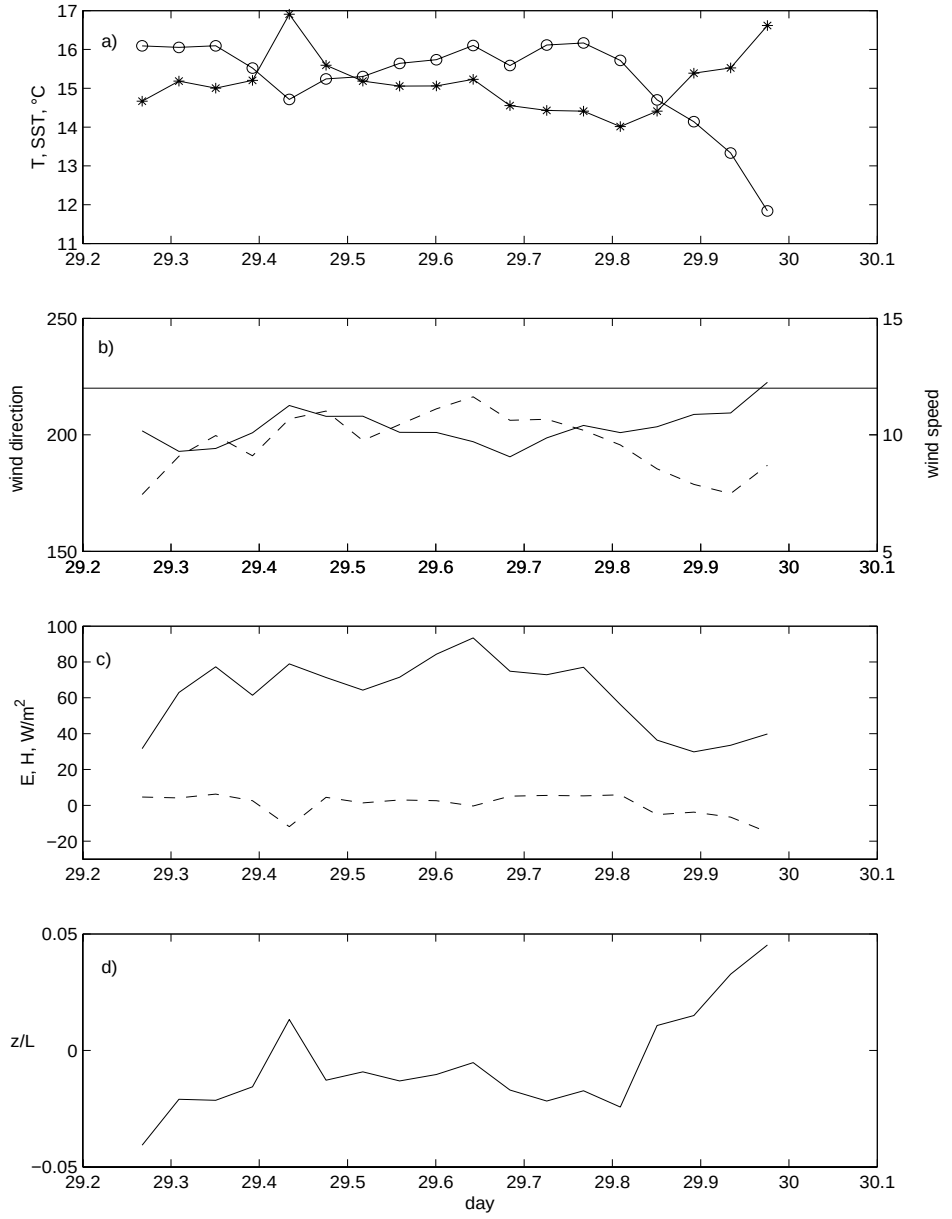

Figure 4.16 Measurements from August 29 of a) SST (circles) and air temperature (stars), b) wind direction (solid line) and wind speed (dashed line), the thin solid line represents the limit of undisturbed wind direction, c) latent heat (solid line) and sensible heat (dashed line) and d) z/L.

4.1.4.1 Stability and heat fluxes

The stability parameters z/L and ΔT (i.e. the difference between the temperature of the atmosphere and the SST) show a good agreement. (See fig. 4.16a and 4.16d). Before the upwelling they both indicate an unstable stratification, but for one data point around 9:40 am (decimal day 29.43) when they both show stable stratification due to a sudden jump in both SST and air temperature. Shortly after the upwelling event has started the stratification becomes stable. It takes a bit longer for this stabilization to show in the

temperature profiles, but these also indicate a neutral or slightly unstable stratification that becomes stable as the SST starts to fall. (See appendix B, fig. B4.)

The co-spectra of w' and T' give a similar result. They indicate a transition from stable to unstable stratification.

The heat fluxes and their bulk calculations are shown in fig. 4.17.

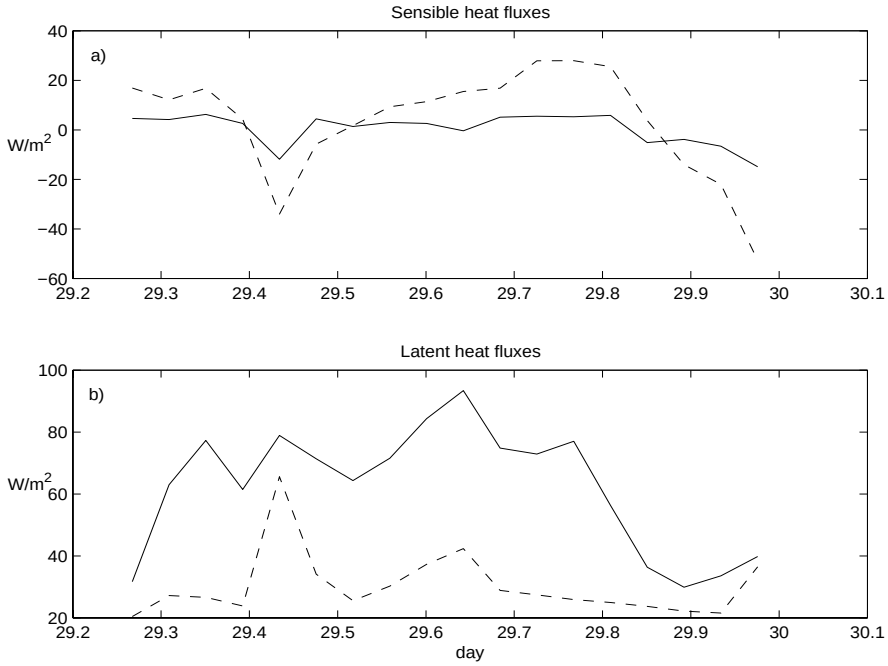

Figure 4.17 a) The sensible heat flux (solid line) and the bulk calculation thereof (dashed line). b) The latent heat flux (solid line) and its bulk calculation (dashed line).

The flux of sensible heat is positive before the upwelling event but as the SST decreases it changes direction, albeit the bulk calculation of the flux gives a much larger decrease than the measurements.

The latent heat flux decreases as the wind speed and the SST decrease. The bulk calculated flux does not show a similar behaviour. The bulk calculation underestimates the flux and does not show any significant decrease as the SST decreases.

The co-spectra of w'q' show that the flux is dampening during the upwelling. The same increase at the very end of the measurement period that shows in the bulk calculation and the measurements is also present in the co-spectra. (See fig 4.18.) The energy spectra of q is dampened during the upwelling and no increase towards the end can be observed here.

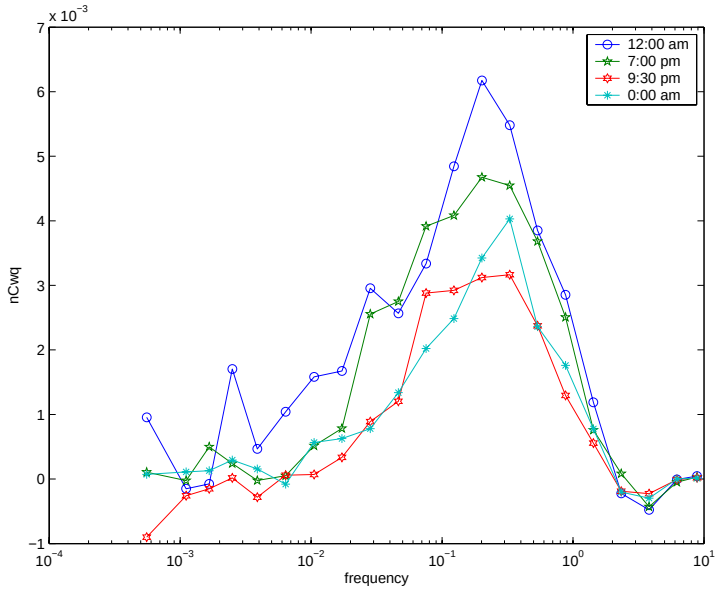

Figure 4.18 The co-spectra of w'q' on Aug 29.

4.1.4.2 Flux of CO_2

As the upwelling event starts the difference in CO_2-levels between the atmosphere and the sea diminishes therefore the flux of CO_2 decreases. (See fig. 4.19.)

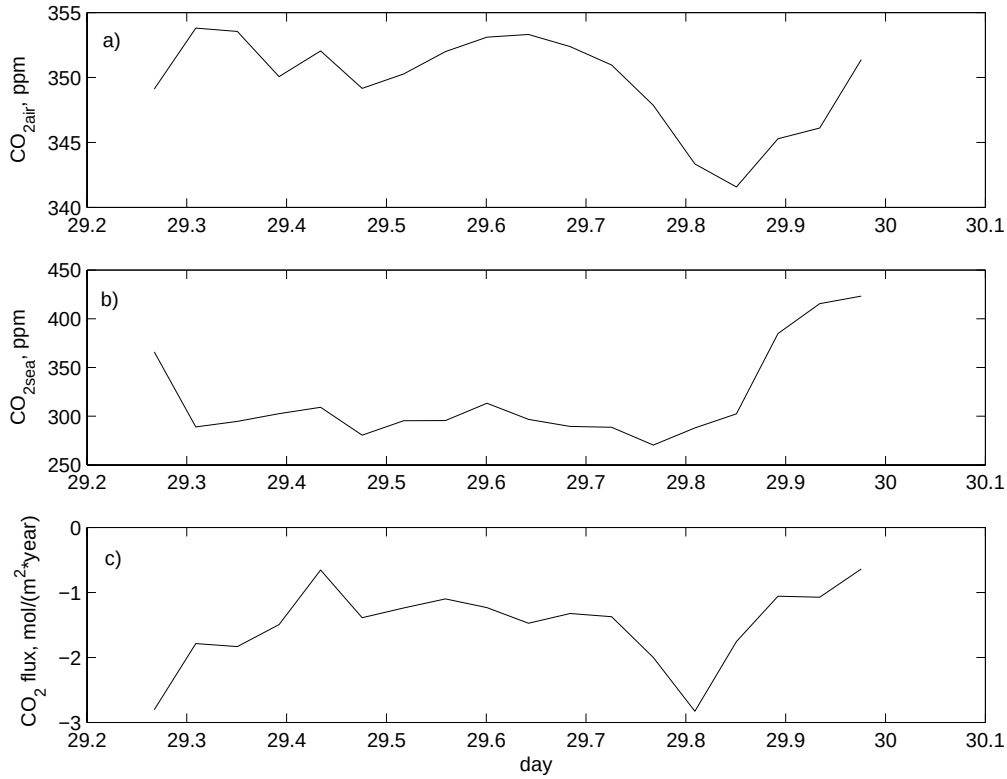

Figure 4.19 The CO_2 measurements from August 29, a) the amount of CO_2 in the air, b) the amount of CO_2 in the sea and c) the flux of CO_2.

The bulk calculations of the CO_2-flow overestimates its magnitude. (See fig. 4.20.) A clearer correlation with the measurements can be observed if the amount of CO_2 in the ocean is raised artificially with 37 ppm. The major disagreement between the measured flux and the calculated ones is that while the measurement shows a negative flux that is decreasing, both bulk calculations give a positive flux when the upwelling has started, about the same time as the stratification turns stable.

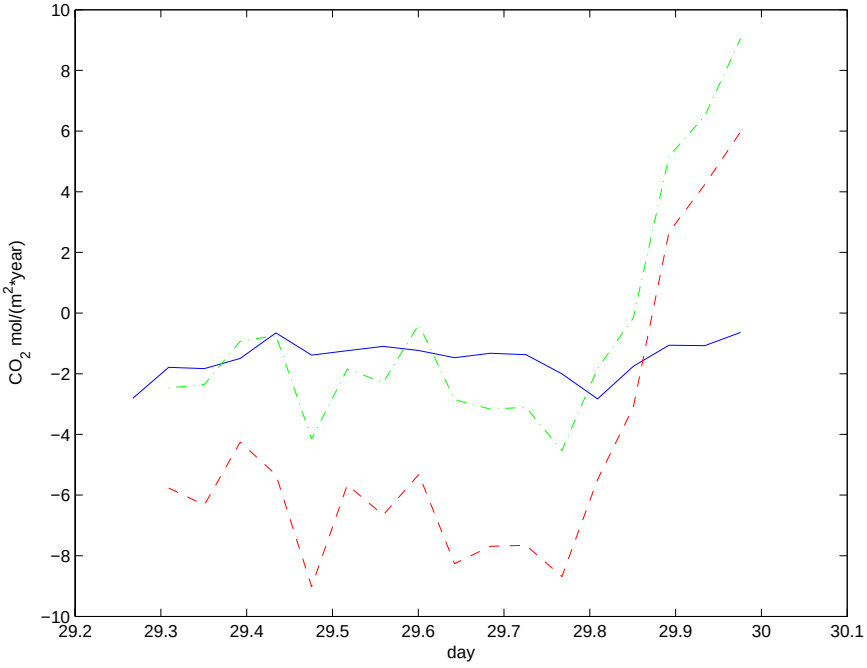

Figure 4.20 Two different bulk calculations on Aug 29. The solid line represents the measurements, the dashed line the bulk calculation using the measurements and the dashdotted line the bulk calculation when the CO_2 in the sea surface is artificially increased with 37 ppm.

Both spectra and co-spectra are also decreasing. (See fig 4.21.) This supports the measurements, the flux is approaching zero, but never turns into a positive flux.

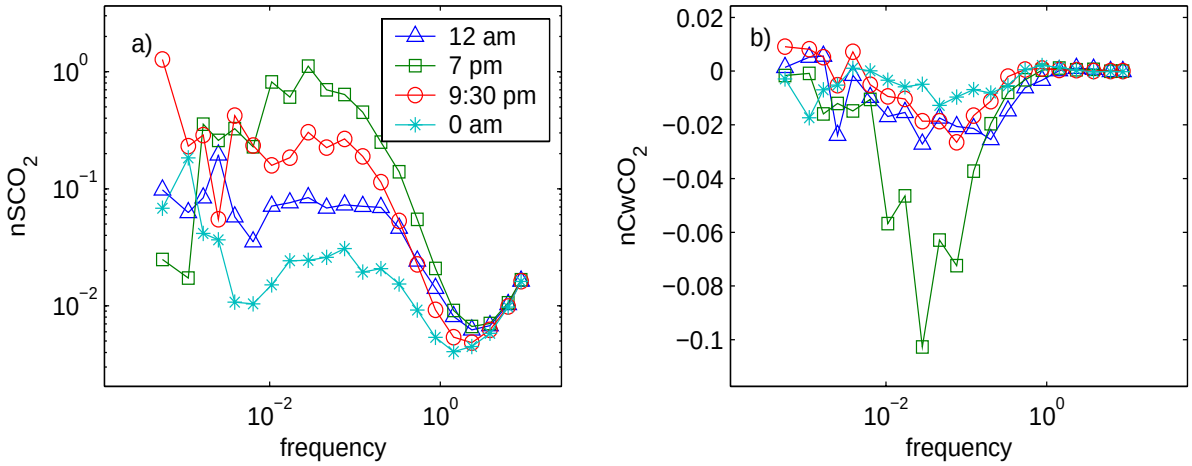

Figure 4.21 a) The energy spectra and b) the co-spectra of CO_2 on Aug 29.

4.2 Fluxes of CO_2

The air-sea flux of CO_2 is by a large degree explained by the difference in the concentration of CO_2 between the atmosphere and the sea. When, as is usually the case in these data, the concentration of CO_2 is larger in the air than in the sea the flux is supposed to be directed downwards. An upwelling event will bring CO_2-rich bottom-water to the surface so the flux decreases and may also change sign. When the difference between the concentration of CO_2 in the atmosphere and the sea increases the air-sea flux of CO_2 should also increase. (See fig. 4.22.) This relation is observed on Aug 29 (stars) and July 12 (circles). July 15 (diamonds) there is a less clear correlation between the flux and the CO_2-difference. On June 24 (triangles) a counter-gradient flux is observed. This positive flux also increases as the difference in CO_2-levels increase, contrary to what can be expected.

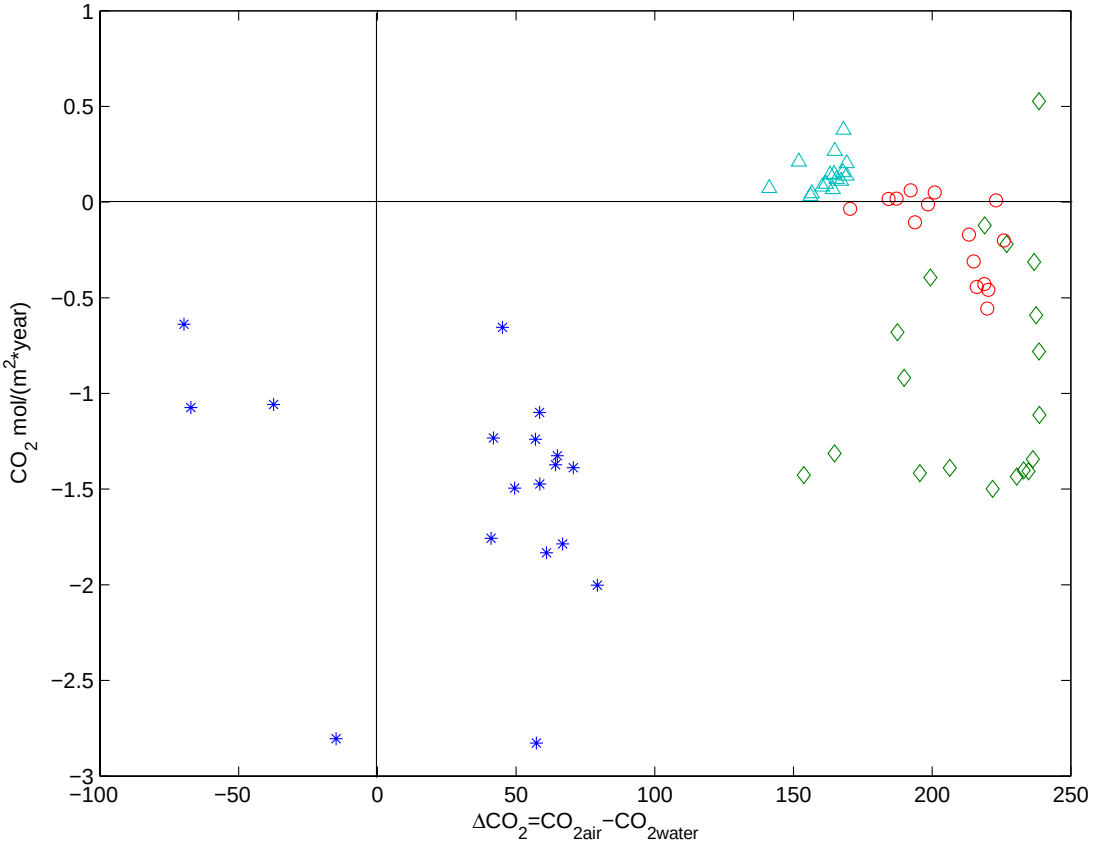

Figure 4.22 The flux of CO_2 relative the difference in the amount of CO_2 between the water and the air. The triangles represent the measurements on June 24, the circles July 12, the diamonds July 15 and the stars Aug 29.

The calculated flux of CO_2 is overestimated for all the measurement periods. This has been discussed in previous sections but figure 4.23 gives a clearer picture as to how large this overestimation is. The best agreement between measured and calculated flux in these measurements is on Aug 29. The calculation still overestimates the flux but not as much

as on July 12 and 15. The counter-gradient flux observed in the measurement on June 24 is not reflected in the bulk calculation.

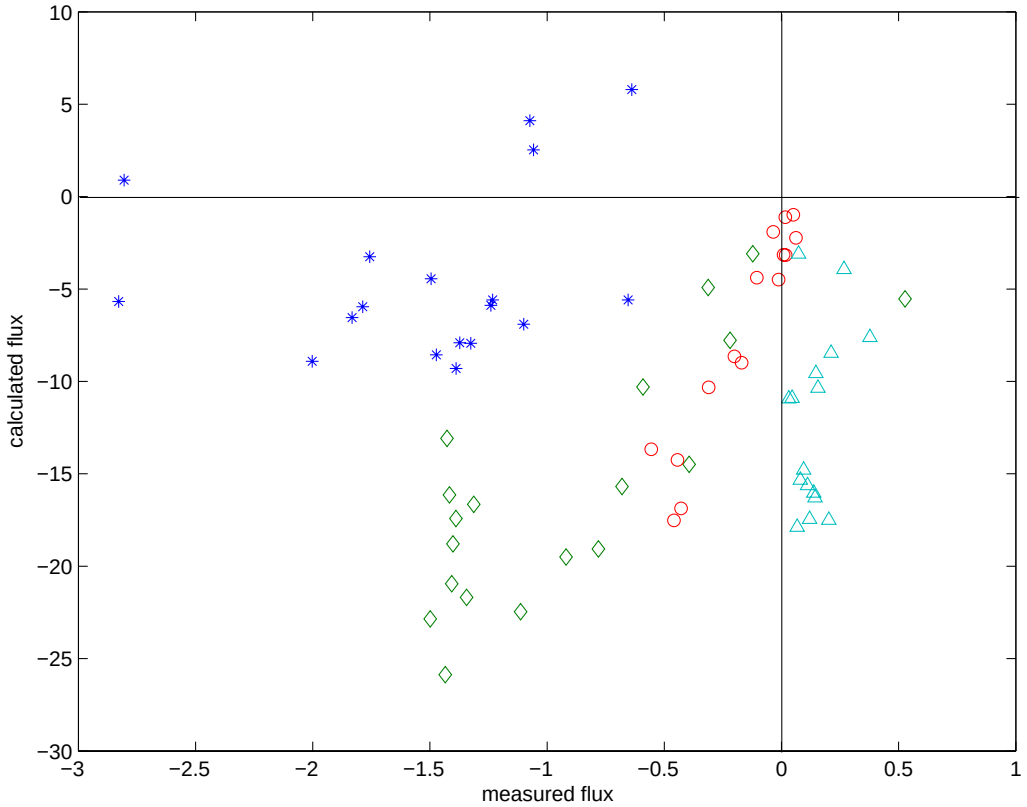

Figure 4.23 The measured flux of CO_2 relative the calculated flux. The triangles represent the measurements on June 24, the circles July 12, the diamonds July 15 and the stars Aug 29. Note the difference in the scale between the x- and the y-axis.

Another factor important for the behaviour of the flux of CO_2 is the wind speed. Generally, the higher the wind speed is the larger is the flux. (See fig. 4.24.) The importance of the wind speed to the flux of CO_2 is seen in the bulk expression for estimating the flux (equations (2.23) and (2.24)). The wind speed in this formula, as opposed to the bulk formulas of latent and sensible heat, is squared. Other formulations of the transfer velocity even use the cube of the wind speed. The relation between the calculated flux and the wind speed is shown in fig. 4.25.

The relation between the wind speed and the flux of CO_2 is more clearly observed on July 12 and July 15 than on June 24 and Aug 29. All of the situations show a decreasing wind as the upwelling event progresses. This decrease in wind speed might help to explain why the flux on June 24 is decreasing, but there is no explanation for the direction of the flux on this day. When regarding all the four periods together the correlation between the CO_2-flux and the wind speed is very clear. As the wind speed increases so does the flux of CO_2.

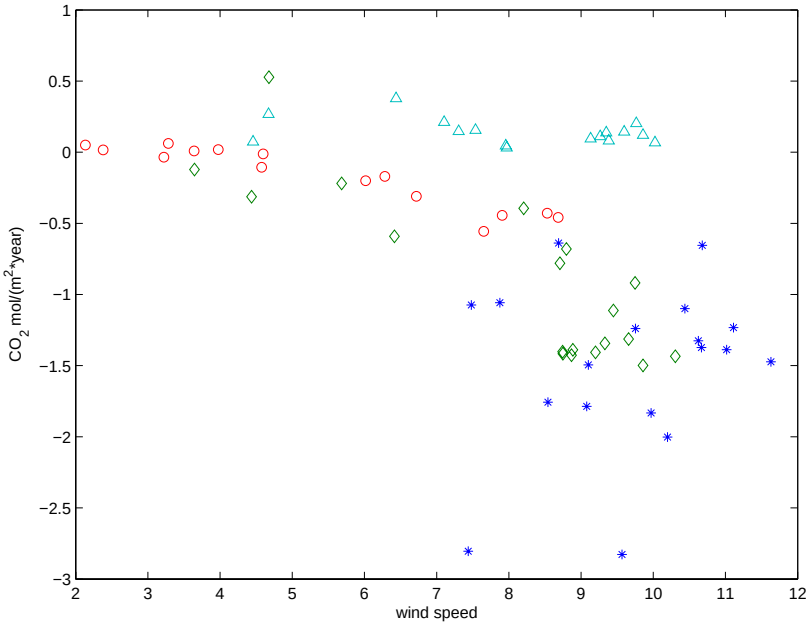

Figure 4.24 The flux of CO_2 as a function of the wind speed. The triangles represent the measurements on June 24, the circles July 12, the diamonds July 15 and the stars Aug 29.

The calculated CO_2-fluxes relative the wind speed are shown in fig. 4.25. The most striking difference between the measured and the calculated fluxes relative the wind speed is that in fig. 4.25 the calculated flux on Aug 29 is smaller while the others agree very well with each other. In fig 4.24 (the measured fluxes) it is the values from June 24 that disagree the most with the fluxes of the other periods

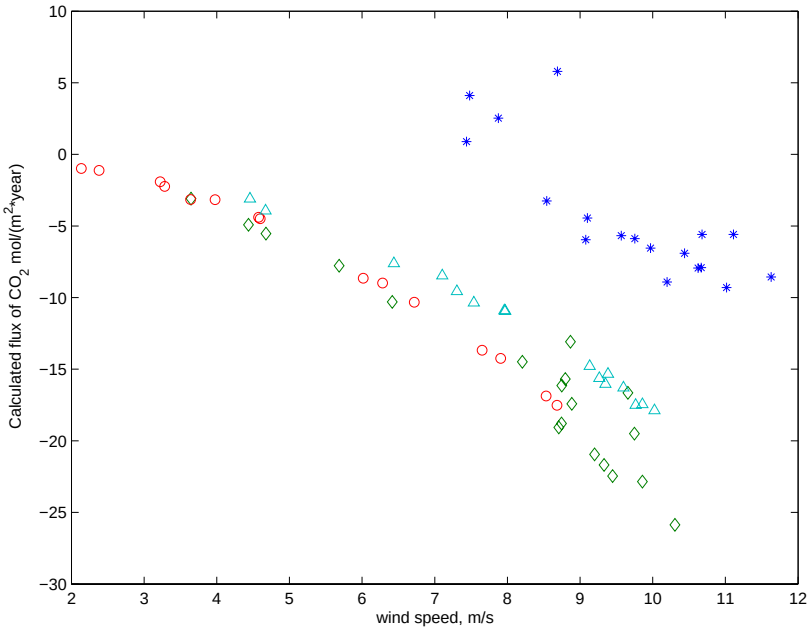

Figure 4.25 The calculated flux of CO_2 relative the wind speed. The triangles represent the measurements on June 24, the circles July 12, the diamonds July 15 and the stars Aug 29.

The flux is also dependent on the stability. (See fig 4.26.) As the stability increases the fluxes should be dampened because the turbulent fluctuations are dampened. The four measurement periods all shows indications of this relation. The relation is clearest during Aug 29. The transfer velocity in bulk formula for calculating the CO_2-flux is not dependent on stratification. These data suggests that a stability dependence should be included in the formula for calculating the CO_2-flux.

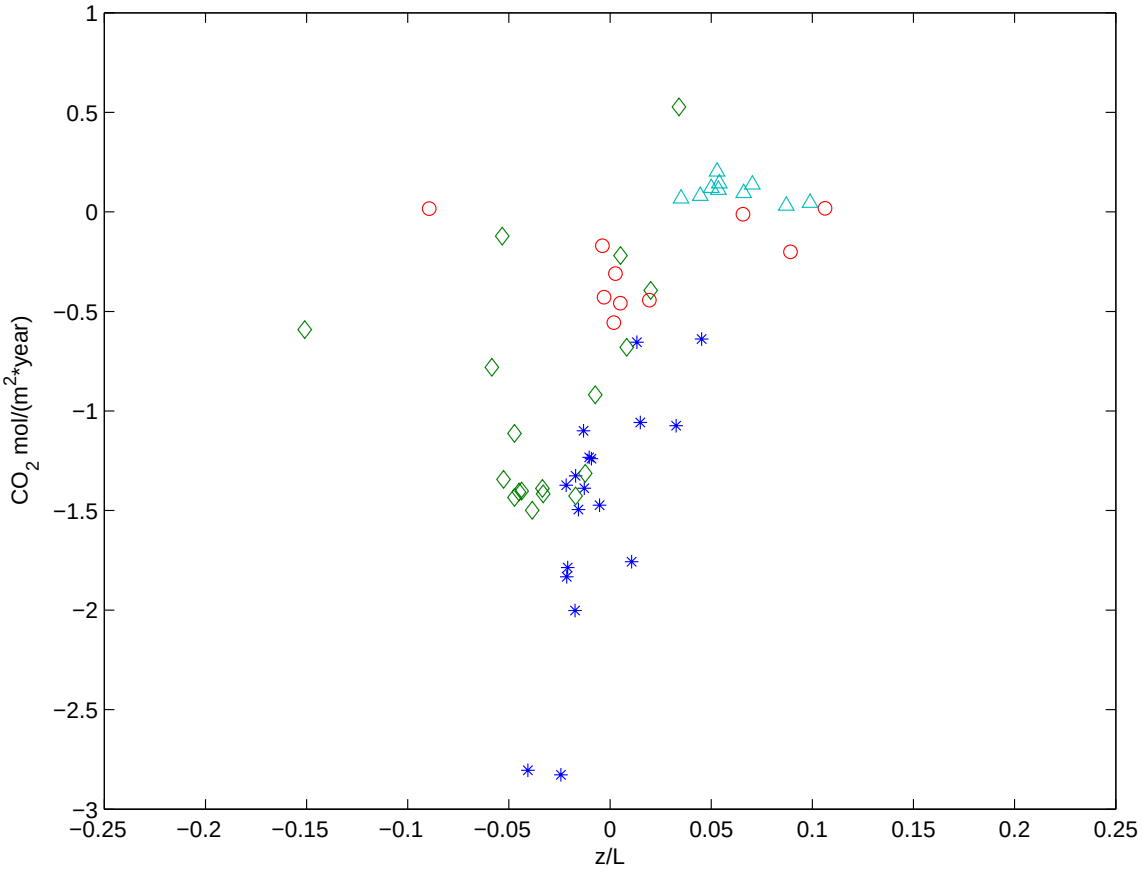

Figure 4.26 The CO_2-flux as a function of the stability parameter z/L. The triangles represent the measurements on June 24, the circles July 12, the diamonds July 15 and the stars Aug 29.

The correlation between a turbulent flux and the stability and the wind speed is also illustrated by the latent heat flux. The latent heat flux show a clear correlation with the stability and the wind speed. (See fig. 4.27.) As the wind speed increases the flux of latent heat also increases. This relation is especially clear on Aug 29. As in the case of the flux of CO_2, the stability has a dampening effect on the latent heat flux.

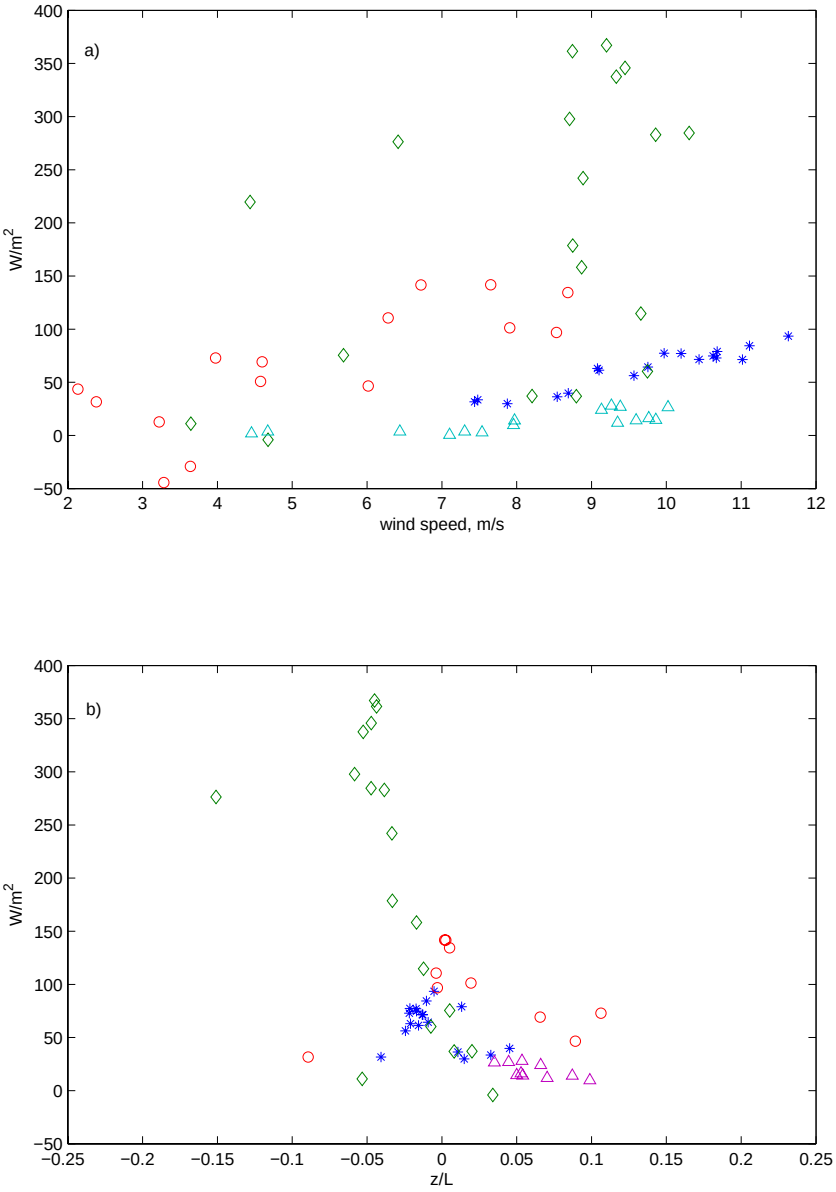

Figure 4.27 The latent heat flux relative a) the wind speed and b) the stability for all four periods. The triangles represent the measurements on June 24, the circles July 12, the diamonds July 15 and the stars Aug 29.

4.3 Manipulated bulk calculations

In an attempt to investigate whether the upwelling events actually reached the flux footprint area the bulk calculations were manipulated so as if the upwelling events never happened. This was done because the measurements from the buoy are perhaps not representative of what happens in the flux footprint area. There is also a possibility that the buoy-measurements, from 5 m below the surface, does not represent the values in the surface water.

The SST was set to be constant (at the value it had before the upwelling event in question) and the same was done for the concentration of CO_2 in the surface water to see which effect this might have on the fluxes.

The flux of latent heat is to a large extent controlled by the difference between the actual level of moisture and the saturation level of moisture. The moisture content of the air is measured 10 m above the water level and the saturation point of the moisture is calculated using the temperature at the same height and the author of this study does not know how to manipulate this so that no upwelling happened.

The effects of the manipulated bulk calculations is most clearly seen in the flux of sensible heat. On July 15 the constant SST gave a calculated flux that agreed better with the measurement before the upwelling. During the actual upwelling event the bulk calculations with the actual values shows an unexpected dip on July 15. This is illustrated in fig. 4.28. The bulk calculation of the sensible heat flux when the SST is set at a fix value agrees considerably better with the measurements of the flux than the bulk calculation where the SST varies according to measurements. The bulk calculation with the real SST shows a strange dip in the flux during the upwelling that does not show when the SST is said to be constant.

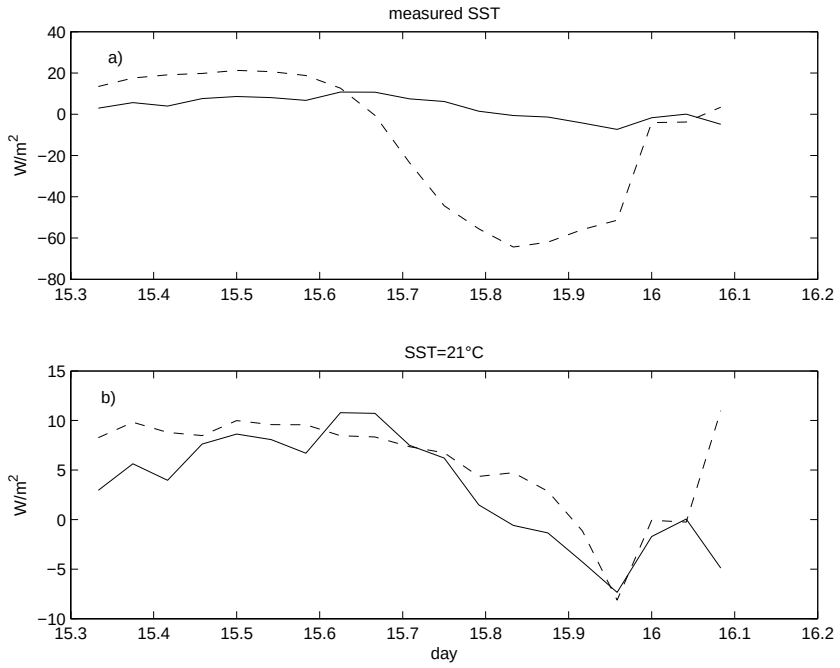

Figure 4.28 a) The measurements of the sensible heat flux (solid line) on July 15 and the bulk calculation of the same flux (dashed line).
b) The measurements of the sensible heat flux (solid line) and the manipulated bulk calculation (dashed line) where the SST is set to be constantly 21°C.

The artificially constant CO_2-levels in the surface water does not influence the bulk calculations of the CO_2-flux as much as the constant SST influences calculations of the sensible heat flux.

The difference between the manipulated CO_2-flux and the bulk calculation using the actual values on July 15 is illustrated in fig 4.29. The two calculations agree very well with each other before and after the upwelling event even though there is a large difference between the calculated and the measured fluxes. The calculation using the actual values agrees better with the measurements. It is strange that the sensible heat flux for the same period is better described by the manipulated bulk calculation while the CO_2-flux is better described by the calculation using the actual values.

The manipulation of the latent heat flux shows little or no difference to the bulk calculations using the measurements due to the reasons discussed above. Presumably this is also because the latent heat flux depends mostly on the wind speed. What little difference between the calculations that can be observed shows that the calculations using the proper values of SST agree better with the measurements.

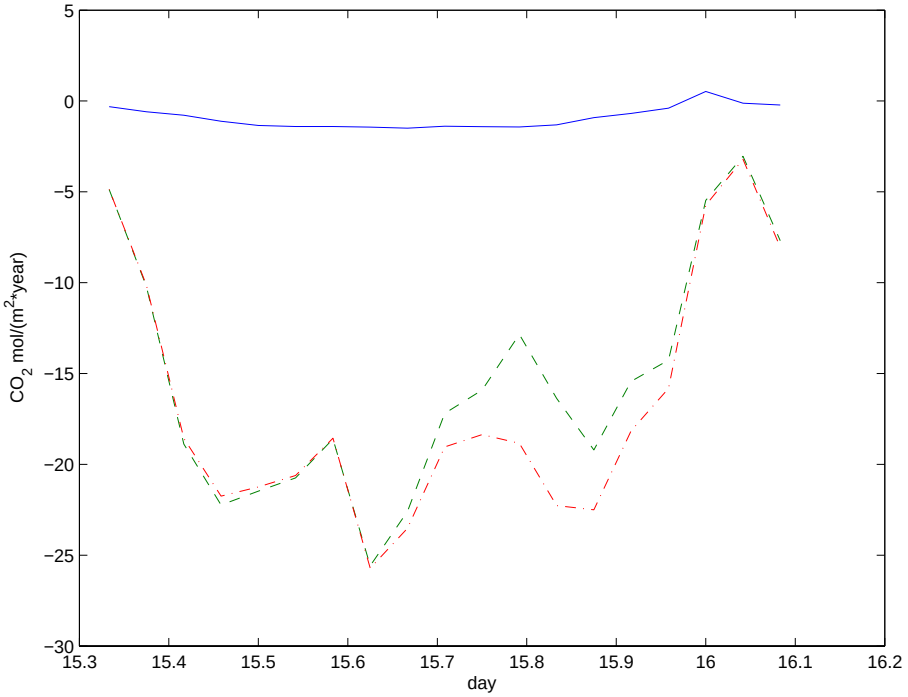

Figure 4.29 The flux of CO_2 on July 15. The solid line represents the measurements, the dashed line the bulk calculation using the measurements and the dotdashed line shows the bulk calculation using a constant SST and CO_2-level in the surface water.

5 Discussion

The analysed data does not give an entirely conclusive picture of what effects an upwelling event has on the atmosphere. Given that the situations are rather complex this is not unexpected.

Footprint area

The question is whether the measurements from the CO_2-buoy are representative of what the tower measures. During the upwelling events in this study the wind direction is from southwest to south-southwest which means that the footprint area of the tower lies in this direction. The CO_2-buoy, however, is moored 1 km south-southeast of the tower. As discussed before, Smedman et al. (1999) investigated the wave field at the same site, but considered their wave-rider buoy moored 4 km southeast of the tower to be representative of the wave field in the footprint area. Perhaps the variation of CO_2 in the surface water is less uniform.

The lateness in the stability changes of z/L and the co-spectra of w'T' when compared to the difference in temperature between atmosphere and sea surface on July 15 can give an indication that the measurements from the tower do not correspond to what is happening in the area around the CO_2-buoy. There can be a time delay between when the upwelled water reaches the buoy and when it reaches the footprint area. This would be an explanation as to why the manipulated bulk calculation of the sensible heat flux using a constant SST agrees better with the measurements than the bulk calculation using the actual values. The time delay may also explain why the flux of CO_2 does not change its direction when the SST is increasing but when it is back at its former value. A similar relationship is seen in the latent heat flux, which continues to decrease when the SST is increasing after the upwelling event. The latent heat flux does not start its increase until the SST is back to the values it had before the upwelling event. On the other hand this small increase in the latent heat flux may have more to do with the small increase in wind speed observed at this time.

The upwelling event on Aug 29 is also supported by the satellite image of SST from the morning of Aug 30, figure 5.1. The buoy shows a large upwelling event that starts in the evening of Aug 29 and is not over until midday on the 30th. Due to the change in wind direction the whole situation cannot be studied using the measurements from the tower for reasons discussed previously. The clouds cover Östergarnsholm but considering the low temperatures that indicate an upwelling event all along the southern part of the east coast of Gotland it is reasonably to assume that the sea around Östergarnsholm also is a part of it.

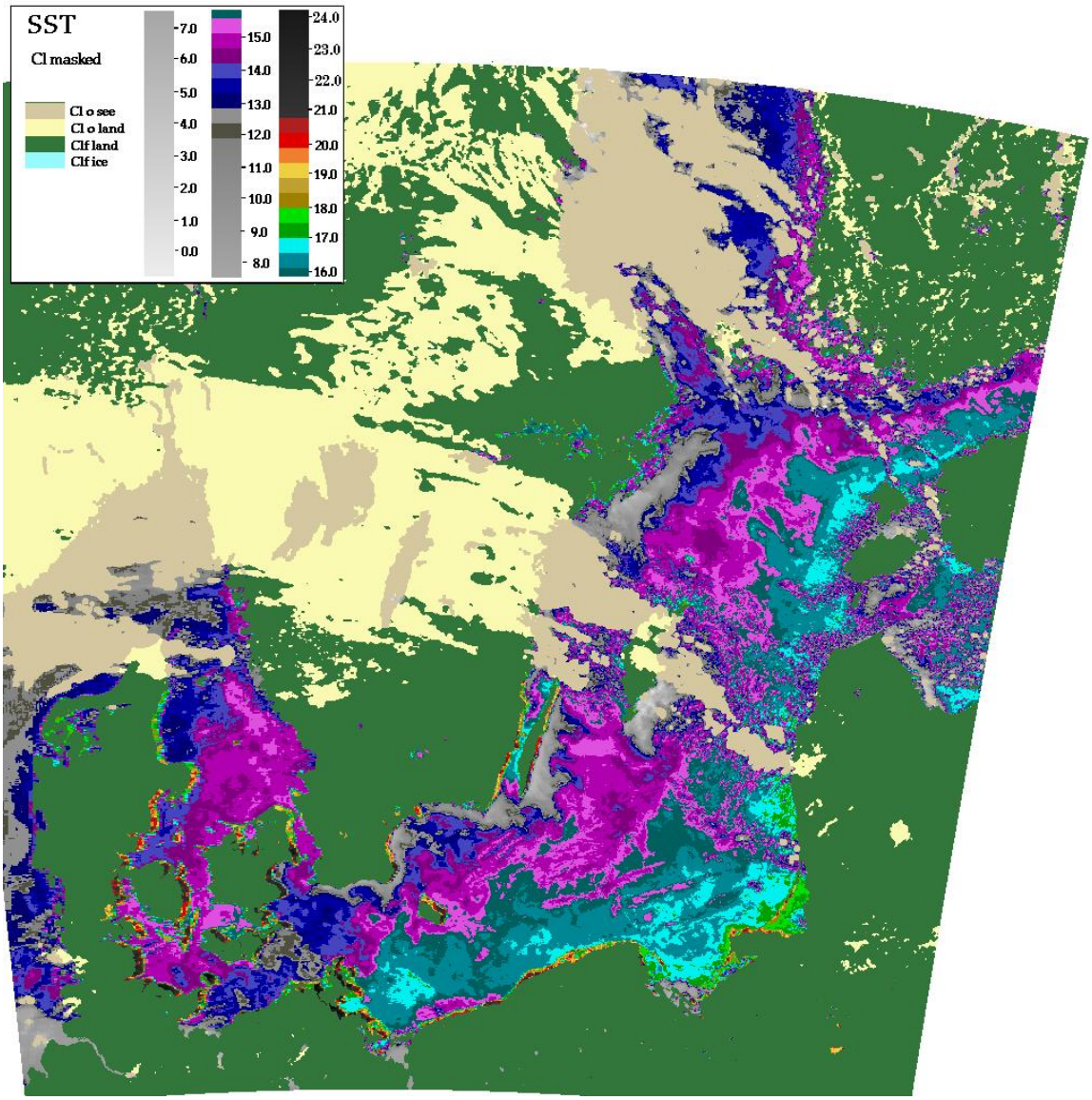

Figure 5.1 A satellite image of the SST in the morning of Aug 30. Unfortunately there is a cloud cover above Östergarnsholm but the low SST along the southern part of the east coast of Gotland suggests that this upwelling extends to the water around Östergarnsholm as well.

Other effects on the air-sea exchange of CO_2

The level of CO_2 in the sea is not only controlled by the temperature and biological factors. The salinity also effects the solubility of CO_2. Thomas and Schneider (1999) investigated the seasonal cycle of CO_2 in the Baltic Sea surface waters and drew the conclusion that the salinity had a larger effect on the changes of dissolved inorganic

carbon[3] in the surface water than the new production and remineralisation of organic matter. This is the main difference between the Baltic Sea and the oceanic carbonate system. The water in the Baltic Sea is brackish. The surface waters east of Gotland have an average salinity of 7 psu (Omstedt and Hansson, 2006) while the average value for sea water is 35 psu, (Pinet, 2003).

Even though this study does not investigate the effects of phytoplankton on the air-sea exchange of CO_2 it is vital to remember that this also affects the flux. The plankton live mostly at or very near the surface. Their photosynthesis reduces the concentration of CO_2 in the surface water. This results in a vertical variation in the concentration of CO_2 and as the buoy measures the CO_2-levels at the depth of 5 m this is a possible source of error in the estimations of the CO_2-flux.

An upwelling event brings nutrient-rich bottom water to the surface and this should increase the primary production. The Baltic Sea is suffering from eutrophication so if even more nutrients are added to the surface waters this would probably not cause an increase in primary production.

It should also be noted that the time scale of the increase in primary production due to an upwelling event (if indeed the upwelling event has any effect here) is longer than 12 hour. This time limit is the longest measurements during an upwelling event in this study. It is the time it takes from that the upwelling event starts on July 15 till the wind direction changes to above the limit so the measurements from the tower can no longer be used. Assoc. Prof. Ulf Larsson of the Department of System Ecology, Stockholm University states that that the time needed for the phytoplankton to respond to the changes in nutrient levels is one to several days depending on the water temperature. Thus increased primary production as a result of an upwelling event can be ruled out as a possible source of error in the measured air-sea flux of CO_2.

[3] Only a small part of the CO_2 in the ocean is solved as a gas. Most of it has reacted chemically with the water and is in the form of carbonic acid (H_2CO_3), bicarbonate ions (HCO_3^-) or as carbonate ions (CO_3^{2-}). At equilibrium the relative proportion of the carbon species depends on the pH of the water. At pH-levels that are normal for sea water bicarbonate ions are responsible for 80% of the carbon species. If the water is more acidic there will be a higher concentration of CO_2. If it is more basic the amount of carbonate ions will increase.

6 Conclusions

It is almost impossible to quantify the effects of an upwelling event on the atmosphere from the data available in this study. Trends are observed but the actual impact of the upwelling is difficult to determine.

The data indicate that the assumption of the stabilizing atmosphere and the reduced turbulent fluxes is correct. In all four cases a stabilization of the atmosphere is observed. The size of the stabilization differs and the different stability parameters are not always in exact agreement with each other.

When the atmosphere is stabilizing the turbulence is reduced and as a consequence the turbulent fluxes must also decrease. It is interesting to note that the flux of CO_2 also shows this effect.

The sensible heat flux is decreasing in two of the cases as expected, Aug 29 and July 15. What is causing the increase in the sensible heat flux on July 12 is quite inexplicable as the wind simultaneously decreases and a larger difference between the temperature of the atmosphere and the SST should cause a larger negative flux, not a positive one as is observed. There is, however, no increase in the magnitude of the flux. The insignificant changes in the sensible heat flux on June 24 are probably more due to changes in wind speed and stability than temperature differences between the sea and the atmosphere.

The decrease of the latent heat flux is observed in all four cases. As the SST goes down so does the flux of latent heat.

Because the amount of CO_2 in the atmosphere is greater than the amount in the sea surface waters the flux of CO_2 should be negative. The flux is approaching zero as a result of all the upwelling events. In three of the situations in this study the flux is behaving according to theory and approaches zero from the negative direction. On June 24, however, there is a counter-gradient flux. The flux of CO_2 is approaching zero from the positive direction despite the fact that the amount of CO_2 is larger in the air than in the sea.

Given that the situations are rather complex it is difficult to understand which changes in the atmosphere that were caused by the upwelling events and which were due to other factors. The manipulations of the bulk calculation discussed in a previous section was also an attempt to separate them. The SST was set to be constantly at the value it had before the upwelling event started. The same was done for the amount of CO_2 in the surface water. In most of the cases the bulk calculations using the actual values of the SST and the CO_2-levels agreed better with the measurements.

When the manipulated bulk calculations agree better with the measurements, it is probably a consequence of the position of the CO_2-buoy, which is not situated within the flux footprint area and perhaps not always representative of what happens there. During the upwelling event of July 15 the upwelling reaches the buoy earlier than it reaches the

footprint area. This can be the reason why the manipulated bulk calculation of the sensible heat flux agreed better with the measurements than the calculation using the actual values. The manipulated calculation of the CO_2-flux, however, agrees less with the measurements than the calculation using the actual values. On the other hand, both of the calculated fluxes of CO_2 are greatly overestimating the flux.

The most certain conclusion that can be drawn from this investigation is that more measurements are needed. These are needed in order to investigate the effects of upwelling on the turbulent fluxes in detail and to assure that the effects observed in this study are indeed the effects arising from the upwelling of colder deep-water and not due to some other factor that has been overlooked here. It would also be interesting to study the duration of the effects and their vertical extent.

Acknowledgements

First and foremost I would like to thank my supervisor Anna Rutgersson Owenius for all her invaluable help in the completion of this thesis. I would also like to thank the rest of the staff at the Department of Meteorology for their help, especially Ann-Sofi Smedman, Hans Bergström and Cecilia Johansson.

Furthermore I wish to thank Bertil Håkansson and Martin Hansson, SMHI, for the satellite images of SST, and Ulf Larsson and Sven Fransén for their help in unravelling the mysteries of the lifecycle of phytoplankton.

A big thank you also to my fellow students for being there, to my mother for the front page photo and to all the people at Uppsala Ju-jutsu Club for helping me to relax and think about other things than this thesis.

References

Álvarez, Marta, Emilio Fernández, Fiz F. Pérez, 1999, *Air-Sea CO_2 fluxes in a coastal embayment affected by upwelling: physical versus biological control*, Oceanologica acta, vol. 22, no. 5, p. 499-515

Andersson, Leif G., 2003, *The Marine Carbonate System*, Compendium, Department of Chemistry, Göteborg University

Astor, Y.M., M.I. Scranton, F. Muller-Karger, R. Bohrer, J. Garcia, 2005, *fCO_2 variability at the CARIACO tropical coastal upwelling time series station,* Marine Chemistry, vol. 97, p. 245-261

Le Borgne, Robert, Richard A. Feely, Denis J. Mackey, 2002, *Carbon fluxes in the equatorial Pacific: a synthesis of the JGOFS programme*, Deep-Sea Research Part II, vol. 49, p. 2425-2442

Gago, J., M. Gilcoto, F.F. Pérez, A.F. Ríos, 2003, *Short-term variability in fCO_2 in seawater and air-sea CO_2 fluxes in a coastal upwelling system (Ría de Vigo, NW Spain)*, Marine Chemistry, vol. 80, p. 247-264

Hales, Burke, Taro Takahashi, Leah Bandstra, 2005, *Atmospheric CO_2 uptake by a coastal upwelling system*, Global Geochemical Cycles, vol. 19 GB1009

Högström, Ulf, Ann-Sofi Smedman, 1989, *Kompendium i atmosfärens gränsskikt, Del 1. Turbulensteori och skikten närmast marken*, Geotryckeriet, Uppsala, andra reviderade upplagan

Larsson, Ulf, associate Professor, Department of System Ecology, Stockholm University personal communication, April 2006.

Liebethal, Claudia and Thomas Foken, 2003, *On the significance of the Webb correction to fluxes*, Boundary-Layer Meteorology, vol. 109, p. 99-106

Omstedt, Anders and Daniel Hansson, 2006, *The Baltic Sea ocean climate system memory and response to changes in the water and heat balance components*, Continental Shelf Research, vol. 26, p. 236-251

Pinet, Paul R., 2003, *Invitation to Oceanography*, Jones and Bartlett publishers, 3rd edition

Rutgersson, Anna, Ann-Sofi Smedman, Anders Omstedt, 2001, *Measured and simulated latent and sensible heat fluxes at two marine sites in the Baltic Sea*, Boundary-Layer Meteorology, vol. 99, p. 53-84.

Stull, Roland B., 1988, *An Introduction to Boundary Layer Meteorology*, Kluwer Academic Publishers

Smedman A., U. Högström, H. Bergström, A. Rutgersson, K. K. Kahma, H. Petterson, 1999, *A case of air-sea interaction during swell conditions*, Journal of Geophysical Research, vol. 104, no. C11, p. 25,833-25,851

Thomas, Helmuth and Bernd Schneider, 1999, *The seasonal cycle of carbon dioxide in Baltic Sea surface waters*, Journal of Marine Systems, vol. 22, p. 53-67

Tomczak, Matthias, 1996a, *Ekman layer dynamics for shallow seas with stratification*, http://www.es.flinders.edu.au/~mattom/ShelfCoast/notes/chapter03.html, accessed Feb. 24, 2006

Tomczak, Matthias, 1996b, *Upwelling dynamics in deep and shallow water*, http://www.es.flinders.edu.au/~mattom/ShelfCoast/notes/chapter06.html, accessed Feb. 24, 2006

Wanninkhof, R., 1992, *Relationship between wind speed and gas exchange over the ocean*, Journal of Geophysical Research-Oceans 97 (C5), p. 7,373-7,382

The information in footnote 1 came from
http://scienceworld.wolfram.com/chemistry/Fugacity.html, accessed April 4, 2006

Appendices

Appendix A - List of abbreviations and symbols

C_E	the bulk transfer coefficient for latent heat
C_H	the bulk transfer coefficient for sensible heat
d	depth of the frictional boundary layer, in the sea
du/dz	vertical velocity gradient
d_E	depth of the Ekman layer
E	latent heat flux
F	flux of CO_2
f	Coriolis parameter, typically 10^{-4} s^{-1} in the mid-latitudes
g	gravitational constant, 9.81 m/s^2
g/T	buoyancy parameter
H	sensible heat flux, W/m^2
k	von Karman's constant, here 0.4, or the transfer velocity of CO_2
K_0	the solubility of CO_2
L	Monin-Obukhov length
L_v	latent heat of vaporizations
q	moisture, g/kg
Sc	the Schmidt number
SST	Sea Surface Temperature
T	temperature
T_*	scaling temperature
u	wind speed, at 10 m if nothing else is stated
u_*	friction velocity
$\overline{w'T_v'}$	virtual kinematic flux of sensible heat
z	height
θ	potential temperature
λ_m	molecular friction coefficient, kg/(ms)
ν	kinematic molecular viscosity, m^2/s
ρ	density
ρ(t)	autocorrelation function
ω	angular frequency

Appendix B – Temperature profiles

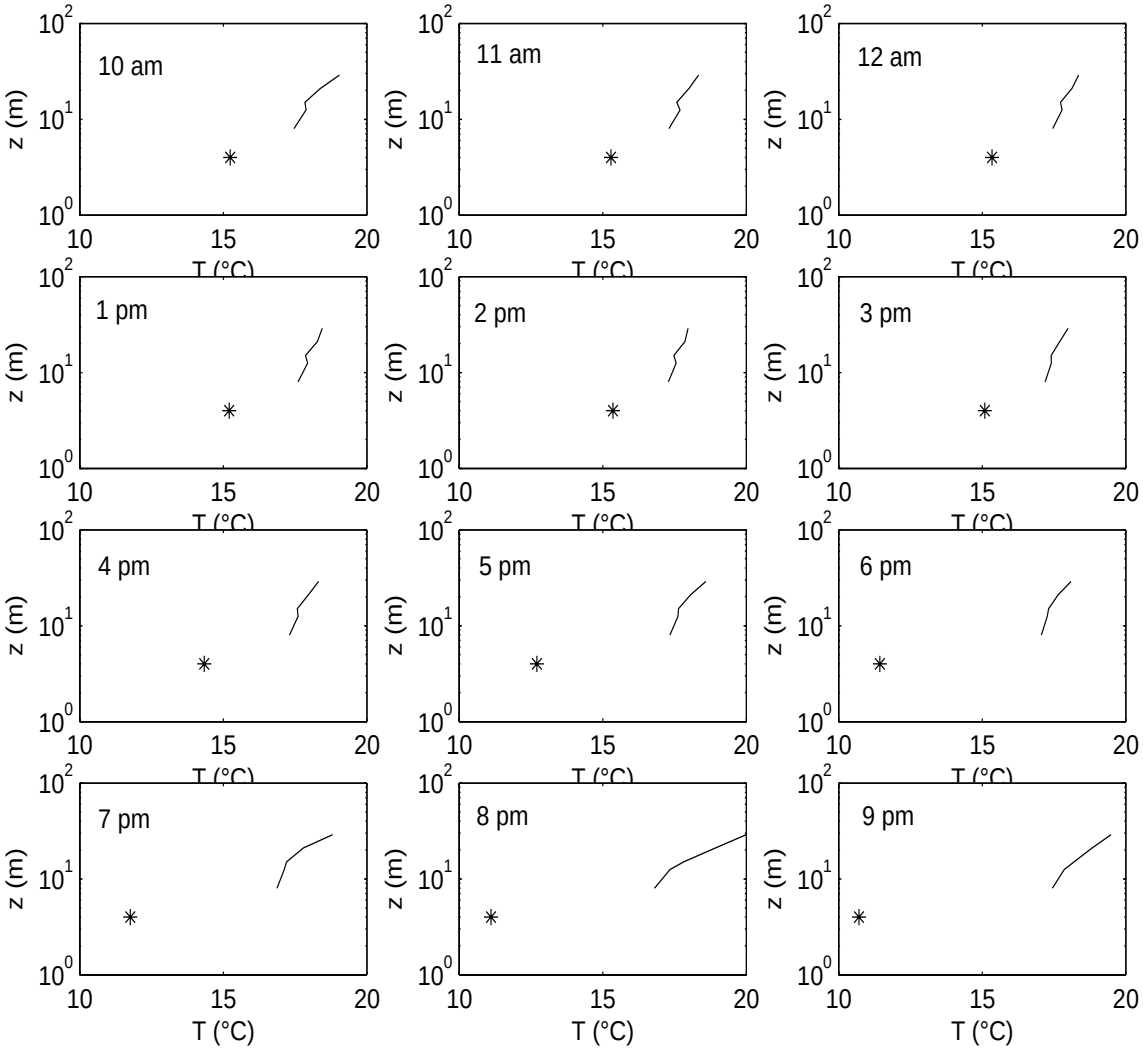

Figure B1 The temperature profile from June 24. The stars represent the SST.

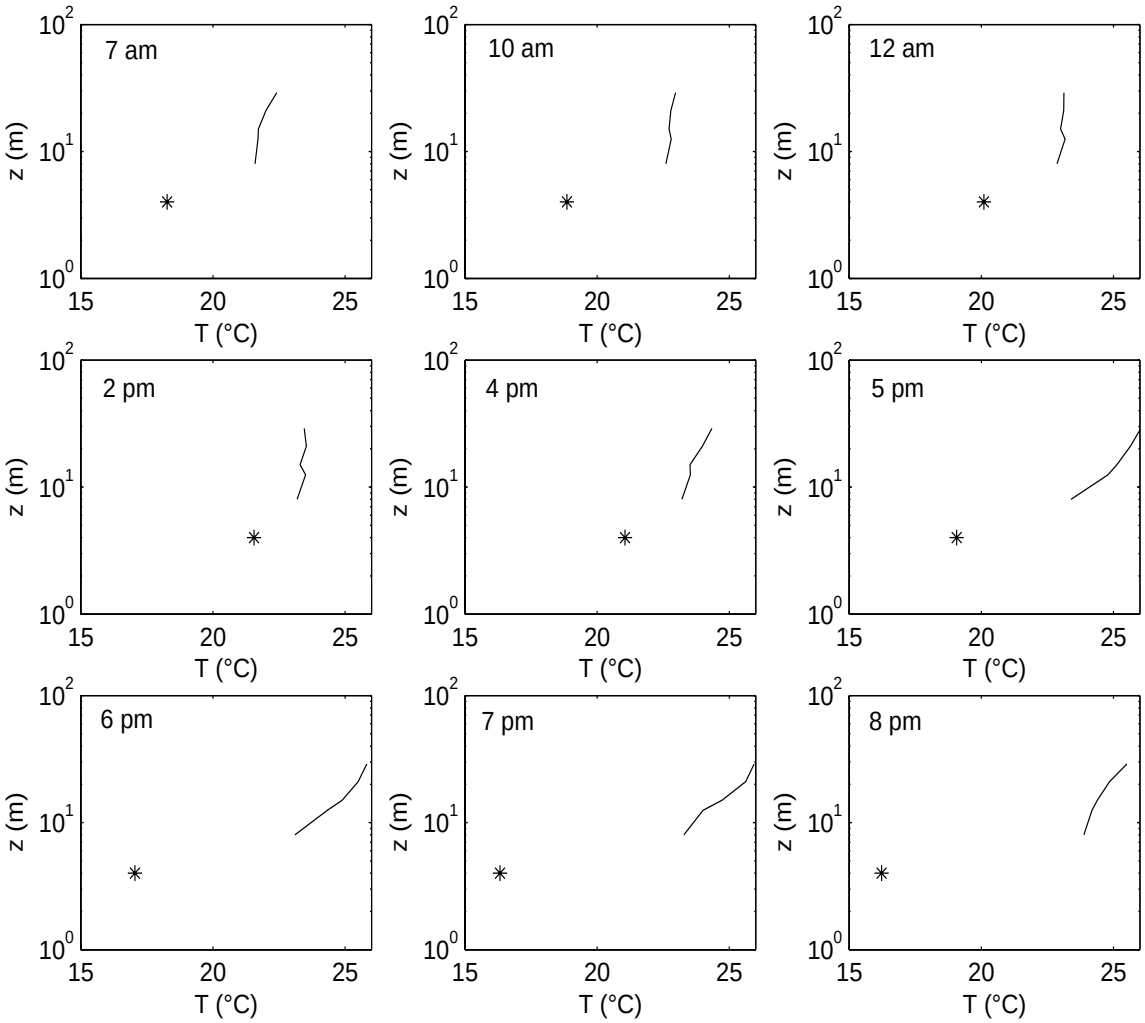

Figure B2 The temperature profile from July 12. The stars represent the SST.

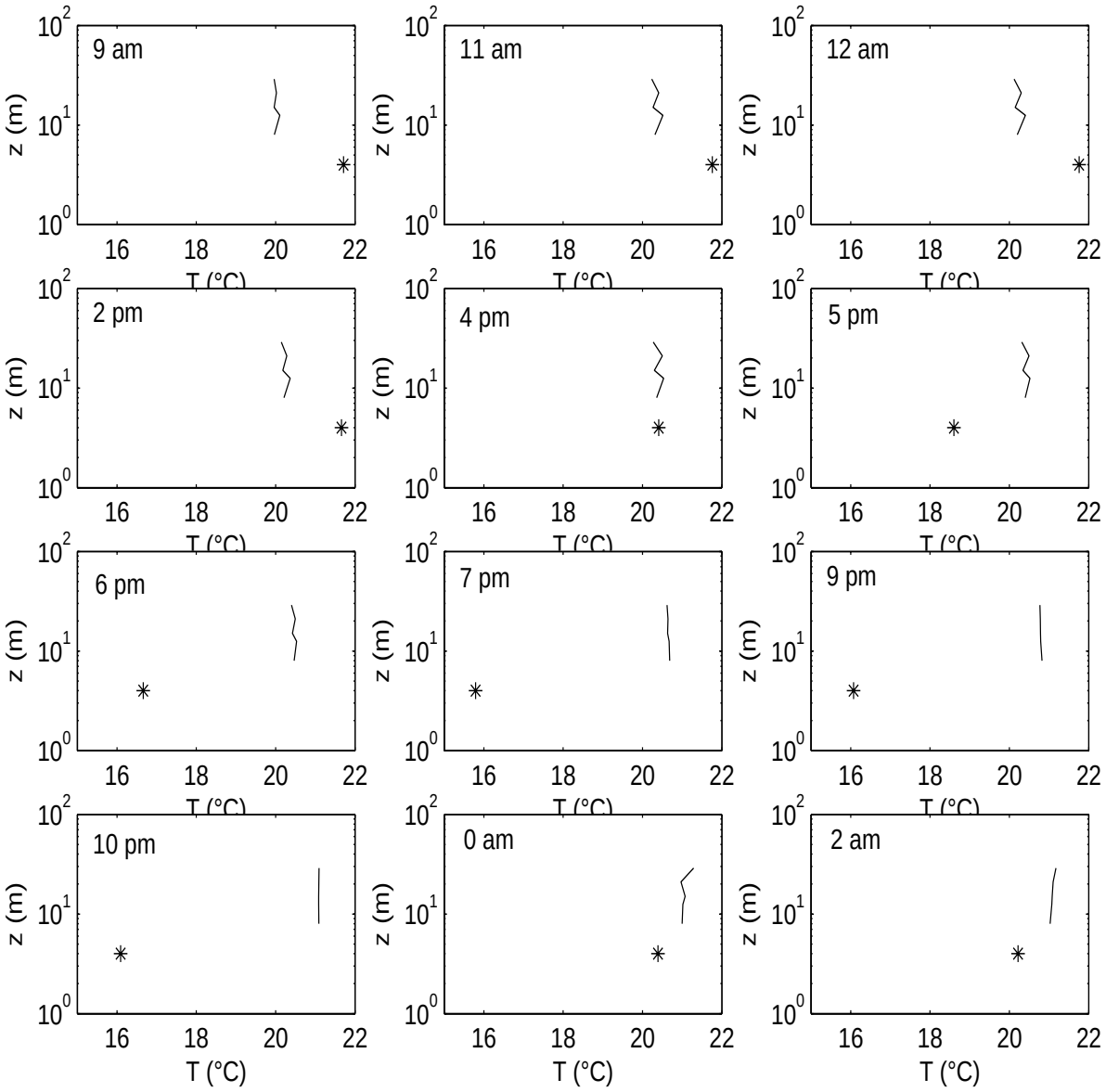

Figure B3 The temperature profile from July 15. The stars represent the SST.

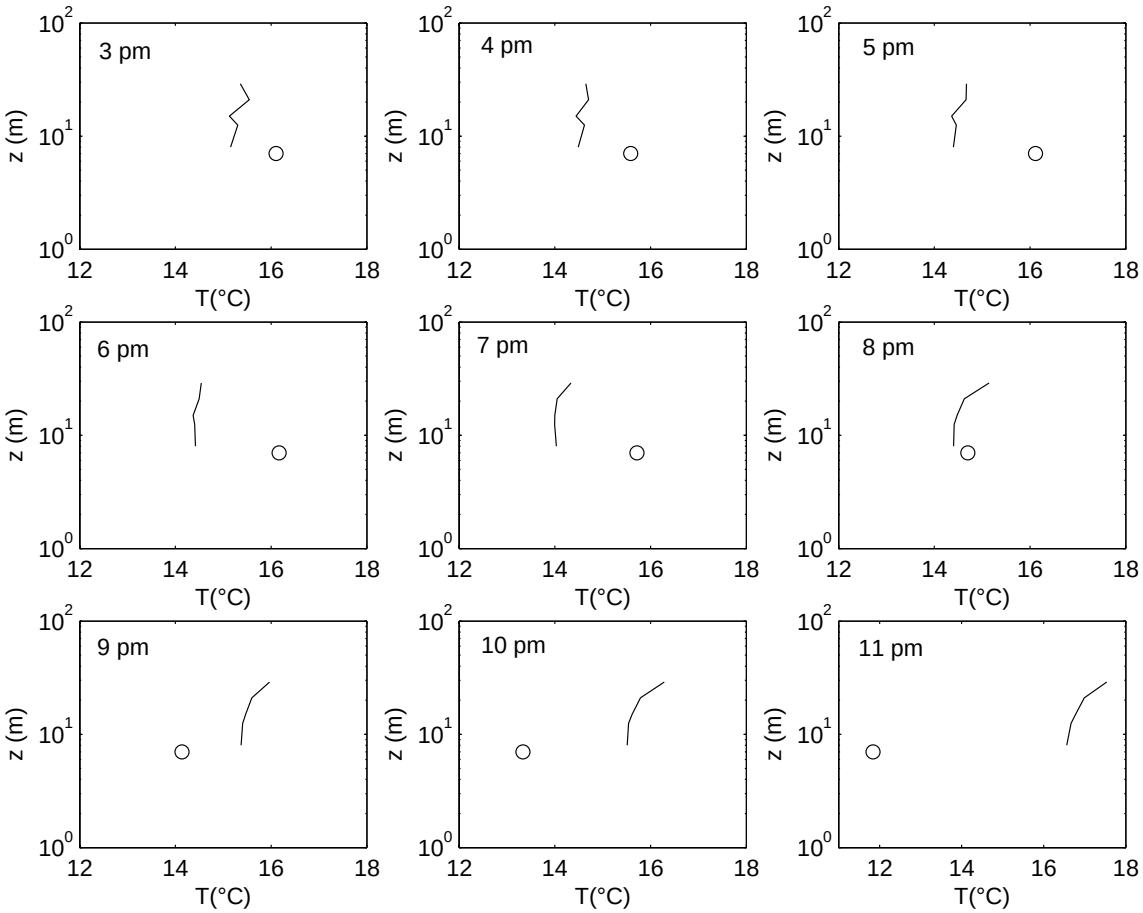

Figure B4 The temperature profile from Aug 29. The circles represent the SST.

Quod potui perfeci.
(I have done what I could.)